Elsevier Editorial System(tm) for Journal of Non-Crystalline Solids

Manuscript Draft

Manuscript Number: NOC-D-20-01120R1

Title: A review of the application of 2D isotropic-anisotropic correlation NMR spectroscopy in structural studies of chalcogenide glasses

Article Type: VSI: Adv. NMR on Glasses

Keywords: Structure, Chalcogenide glass, 2D NMR, Isotropic-Anisotropic correlation NMR

Corresponding Author: Professor Sabyasachi Sen, Ph.d.

Corresponding Author's Institution: University of California, Davis

First Author: Derrick Kaseman

Order of Authors: Derrick Kaseman; Sabyasachi Sen, Ph.d.

Abstract: The application of solid-state high-resolution NMR spectroscopy in the structural investigation of chalcogenide glasses in Ge/As/P/Si-X (X= S, Se,Te) systems has remained challenging even for the spin-1/2 nuclides (29Si, 31P, 77Se, 125Te), owing to their low natural abundance (except for 31P), slow spin-lattice relaxation rate and large CSA and chemical shift distribution induced line broadening effects. However, most of these deleterious effects can be overcome in 2D isotropic-anisotropic correlation NMR experiments, especially when performed at high magnetic field and in conjunction with the Car-Purcell-Meiboom-Gill echo train acquisition. In this contribution we present a short introduction to the basic principles of such experiments and review their applications over the last decade in deciphering short- and intermediate-range structural characteristics of glasses in S-Se, Se-Te, Ge-Se, As-Se and Si-Se systems. We anticipate possible future applications of these 2D NMR experiments in addressing complex structural correlations and distributions in chalcogenide glasses.

Journal of
Non-Crystalline Solids

Confirmation of Authorship

Please save a copy of this file, complete and upload as the "Confirmation of Authorship" file.

As corresponding author, I Sabyasachi Sen, hereby confirm on behalf of all authors that:

1. This manuscript has not been published, was not, and is not being submitted to any other journal. If presented at a conference, the conference is identified. If published in conference proceedings, substantial justification for re-publication must be presented.

2. All necessary permissions for publication were secured prior to submission of the manuscript.

3. All authors listed have made a significant contribution to the research reported and have read and approved the submitted manuscript, and furthermore, all those who made substantive contributions to this work have been included in the author list.

Response to reviewers' comments:

Referee and Editorial Comments:
****

Editor: Probably easiest to improve the figures at this stage than the proof stage--

Reviewer #1: This manuscript on chalcogenide glasses is a nice review on advanced NMR methods to understand short-range structure in these types of glasses. I do not find any issues with the technical content or the way in which this is presented. If a review article of this type is desired for the special issue of JNCS, then I feel this should be published as-is. Since the current review article does not contain any new information/results, it may not be appropriate for the Journal of Non-Crystalline Solids.

The only issue that I found was that some of the figures are of poor quality due to the manner in which they have been reproduced. Please address this issue when submitting any revisions or during the proofing stage

Response: Thank you. We have improved the quality of several figures (Figs. 1,2,3,4,5,6,8,9,16,17) as per your suggestion.

*Abstract

Abstract

The application of solid-state high-resolution NMR spectroscopy in the structural investigation of chalcogenide glasses in Ge/As/P/Si-X (X= S, Se,Te) systems has remained challenging even for the spin-1/2 nuclides (29Si, 31P, 77Se, 125Te), owing to their low natural abundance (except for 31P), slow spin-lattice relaxation rate and large CSA and chemical shift distribution induced line broadening effects. However, most of these deleterious effects can be overcome in 2D isotropic-anisotropic correlation NMR experiments, especially when performed at high magnetic field and in conjunction with the Car-Purcell-Meiboom-Gill echo train acquisition. In this contribution we present a short introduction to the basic principles of such experiments and review their applications over the last decade in deciphering short- and intermediate- range structural characteristics of glasses in S-Se, Se-Te, Ge-Se, As-Se and Si-Se systems. We anticipate possible future applications of these 2D NMR experiments in addressing complex structural correlations and distributions in chalcogenide glasses.

Highlights:

- Application of isotropic-anisotropic correlation 2D NMR
- Review of structure of chalcogenide glasses in S-Se-Te, Ge-Se, As-Se and Si-Se systems

A review of the application of 2D isotropic-anisotropic correlation NMR spectroscopy in structural studies of chalcogenide glasses

[1]D.C. Kaseman and [2]S. Sen

[1]Bioenergy and Biome Sciences Group, Los Alamos National Laboratory,

Los Alamos, NM 87545, USA

[2]Department of Materials Science & Engineering, University of California at Davis,

Davis, CA 95616, USA

Abstract

The application of solid-state high-resolution NMR spectroscopy in the structural investigation of chalcogenide glasses in Ge/As/P/Si-X (X= S, Se,Te) systems has remained challenging even for the spin-1/2 nuclides (^{29}Si, ^{31}P, ^{77}Se, ^{125}Te), owing to their low natural abundance (except for ^{31}P), slow spin-lattice relaxation rate and large CSA and chemical shift distribution induced line broadening effects. However, most of these deleterious effects can be successfully overcome in two-dimensional (2D) isotropic-anisotropic correlation NMR experiments, especially when performed at high magnetic field and in conjunction with the Car-Purcell-Meiboom-Gill (CPMG) echo train acquisition. In this contribution we present a short introduction to the basic principles of such experiments and review their applications over the last decade in deciphering various short- and intermediate- range structural characteristics of chalcogenide glasses in S-Se, Se-Te, Ge-Se, As-Se and Si-Se systems as well as in investigating the molecular dynamics in a P-Se supercooled liquid. We anticipate possible future applications of these 2D isotropic-anisotropic correlation NMR experiments, particularly in conjunction with density functional theory-based calculations of NMR chemical shift tensor parameters and additional signal enhancement schemes, in addressing complex structural correlations and distributions in chalcogenide glasses.

1. Introduction

Chalcogenide glasses constitute an important class of materials that has gained much technological attention and found a wide range of applications in photonics, imaging, sensing and memory devices owing to its infrared transparency, high optical non-linearity and rapid phase change kinetics [1-4]. These glasses are sulfides, selenides or tellurides of group III, IV and/or V elements such as As, Ge, P, Ga and In. The elemental chalcogens S, Se and Te can all be synthesized in amorphous form, however, only Se can be readily quenched into stable bulk glass, while glassy S crystallizes over time at ambient temperature and amorphous Te can only be synthesized as thin films. Although the element Se itself is a good glass-former, it is typical to add elements from group III-V to vastly increase the glass-forming range and capability. The unique compositional flexibility of these glasses in the form of continuous alloying and the structural peculiarities such as formation of homopolar bonds, molecular and other low-dimensional structural units and violation of chemical order are expected to control a wide range of physical properties relevant to various technological applications of these materials. Since S, Se and Te are nominally twofold coordinated in chalcogenides, the structure of glassy Se and Te consist primarily of polymeric $[Se]_n$ or $[Te]_n$ chains, while the structure of glassy S is characterized predominantly by S_8 ring molecules. Increasing addition of Ge, P or As to S or Se results in an increasingly cross-linked network of corner-shared Ge,P $(S,Se)_{4/2}$ tetrahedra or As,P $(S,Se)_{3/2}$ trigonal pyramids[5-11]. On the other hand, over some chalcogen-deficient composition ranges the structure of these liquids may be dominated by homopolar metal-metal bonds (e.g. Ge/As/P-Ge/As/P bonds) and /or molecular units such as As_4S_3, P_4Se_3 and As_4S_4 cage-like molecules[6, 12, 13]. Such structural variation with continuous alloying leads to a wide range of topology and network connectivity (Fig. 1).

Nuclear magnetic resonance (NMR) spectroscopy is one of the most powerful, non-destructive element-specific technique that has been used extensively to investigate the short and intermediate range atomic structure of glasses. The chemical shift, δ, of a nuclide as measured by NMR spectroscopy is highly sensitive to its bonding environment. This second rank tensor can be described using the principal components δ_{xx}, δ_{yy}, and δ_{zz}. The average of these three components δ_{iso} is the isotropic chemical shift:

$$\delta_{iso} = \frac{1}{3}\left(\delta_{xx} + \delta_{yy} + \delta_{zz}\right)$$

These principal components follow the Herzfeld-Berger convention [14] such that:

$$|\delta_{zz} - \delta_{iso}| \geq |\delta_{xx} - \delta_{iso}| \geq |\delta_{yy} - \delta_{iso}|$$

More commonly, the tensor is reported using the isotropic chemical shift and its anisotropy, the latter being characterized by the reduced anisotropy Δ, and the asymmetry parameter, η, defined as:

$$\Delta = \delta_{zz} - \delta_{iso}$$

$$\eta = \frac{\delta_{xx} - \delta_{yy}}{\delta_{zz} - \delta_{iso}}$$

These chemical shift anisotropy (CSA) parameters Δ and η represent the deviation of the tensor from spherical and uniaxial symmetry, respectively. While δ_{iso} of a nuclide is characteristic of its coordination environment, the CSA carries important complementary information related to the symmetry of the local electronic environment of a nuclide and, in combination with δ_{iso}, can

often be useful in deciphering the intermediate-range order in glass structure beyond the nearest-neighbor length scale (*vide infra*).

The application of NMR spectroscopy in the structural investigation of chalcogenide glasses in the Ge/As/P-X (X= S, Se,Te) systems has primarily been limited to the spin-1/2 nuclides ^{31}P, ^{77}Se and ^{125}Te, since NMR of the other quadrupolar nuclides such as ^{73}Ge, ^{75}As and ^{33}S, characterized by either low-gamma and low natural abundance and/or extremely large quadrupolar interaction has remained prohibitively difficult to practically impossible [5-7, 10, 12, 13, 15-25]. Among these, ^{77}Se and ^{125}Te NMR spectroscopy have the unique ability to provide key information regarding the structural and topological evolution in all selenide and telluride glasses as the low-dimensional Se/Te chains transform into a cross-linked 3-dimensional network upon addition of Ge/As/P. However, high-resolution solid-state ^{77}Se and ^{125}Te NMR spectroscopy remain challenging in chalcogenide glasses due to the low natural abundance of these nuclides (~7% each), their long spin-lattice relaxation times, large CSA and chemical shift range, which are particularly problematic for ^{125}Te. The structural disorder in glasses results in large chemical shift distribution in these relatively heavy nuclides causing the isotropic peaks to broaden and overlap. Additionally, the CSA is often too large, even at relatively low magnetic fields, to be averaged via magic-angle-spinning (MAS) at spinning speeds typical of 4 mm and 7 mm MAS probes with sample volumes sufficient to obtain reasonable signal intensity. These issues, compounded by the lowering of sensitivity at relatively low magnetic fields ($\leq$ 7.0 T), result in lengthy data collection and broad and unresolved NMR spectra in the conventional MAS NMR experiment as the spinning sidebands overlap with the broadened isotropic resonances. The overlap affects not only the identification of isotropic peaks, but also impinges on the information that can be learned from the CSA.

Although it is possible to spin samples at speeds fast enough to completely average the CSA, this can only happen at the expense of sample volume and therefore, the signal. The other issue with fast spinning speeds is that the CSA information is completely lost.

Some of these problems can be alleviated quite effectively via the implementation of two-dimensional (2D) techniques where the CSA is separated from the isotropic chemical shift into a correlated second dimension. The isotropic-anisotropic correlation experiment allows the use of high magnetic fields for increased sensitivity and resolution without requiring faster spinning with small sample volume rotors. There are a variety of 2D techniques that have been successfully used to probe the structure of glasses, including Phase Adjusted Spinning Sidebands (PASS), Magic Angle Turning (MAT), Magic Angle Flipping (MAF) and combined techniques such as MATPASS [5, 7, 16, 26-42]. For chalcogenides only the MAT, PASS and the MATPASS techniques have been applied to date, and this review focuses on the basic principles and recent applications of both techniques in the structural studies of these glasses.

2. Basic principles of PASS and MATPASS NMR

2.1. PASS NMR

The PASS NMR experiment was originally proposed by Dixon in 1981 and further developed by Antzutkin et al. [43-45]. The pulse sequence (Figure 2) uses a $\pi/2$ pulse followed by a train of five π pulses. The temporal spacing between the π pulses is based on the PASS equations that have nonlinear, numerical solutions, which depend on the spinning frequency ν_r, and will not be examined in detail here. In each t_1 increment, the spacing between the pulses is adjusted. In this experiment, the phase of the spinning sidebands is adjusted by changing the inter-pulse timings over the course of a rotor period. As the timings are adjusted, the phases of all the sidebands are incremented over 360^o, while the isotropic peaks remain at a fixed phase.

This manipulation results in a separation of the spinning sidebands by their order k in separate rows of a 2D experiment, while a properly sheared projection of the 2D spectrum yields an isotropic spectrum free from any sidebands in the direct dimension i.e. it is equivalent to a high-resolution MAS spectrum at infinite spinning speed that is free of any CSA-related broadening. At any given δ_{iso}, the second dimension will contain a series of sidebands than can be simulated to extract the corresponding CSA parameters. The frequencies of the spinning sidebands for each isotropic position is given by $\delta_{iso}+k\nu_r$ where k represents the sideband order. Thus, the number of PASS t_1 increments multiplied by ν_r must exceed the number of sidebands stemming from the largest CSA. This condition could be difficult to meet in practice in a single PASS experiment for situations where a nuclide is present in multiple environments characterized by a wide range of CSAs. However, as discussed below, the PASS experiment works quite well for nuclides such as ^{31}P in chalcogenides.

2.2. MATPASS NMR

The MAT experiment was invented by Gan in 1992 [46] and was further developed by Grant and co-workers[47], such that, like PASS, MAT has a $\pi/2$ pulse followed by five π pulses. In contrast to PASS, the MAT experiment has the timings of the five π pulses linearly varied with the t_1 increment (Figure 2b). In contrast to PASS, MAT requires more t_1 increments, leading to time-consuming experiments, and a double affine shearing transformation must be used to obtain the isotropic-anisotropic correlation. It was realized by Hung et al. in 2010 [48] that the π-pulse timings in PASS and MAT were related in the t_1 dimension and that by shifting the MAT acquisition time the two experiments could be combined. Consequently, the MATPASS

technique was developed, which combined advantages from each technique, as it uses the linear timings between the π pulses from MAT, but with the reduced t_1 increments and straightforward processing of PASS. Thus, the same experimental considerations for the PASS technique (ν_r and t_1 steps) can be used for MATPASS.

In the case of nuclides with low natural abundance such as ^{77}Se and ^{125}Te, MATPASS with Car-Purcell-Meiboom-Gill (CPMG) echo train acquisition [49, 50] (typically 16-32 echoes) can reduce the data collection time significantly. This echo train acquisition may be appended to the end of the pulse sequence as a series of π pulses, evenly spaced with alternating phase to refocus the spins undergoing T_2-decay to form an echo in between the π pulses, thereby maximizing the amount of signal that can be obtained in a single experiment. The details of applying and processing echo train acquisition for PASS and MATPASS experiments are beyond the scope of this review, but has been discussed in excellent detail by Walder et al.[41]. A distinct advantage of the MATPASS/CPMG technique compared to PASS/CPMG is that it avoids the $1/\sqrt{2}$ loss in sensitivity, making MATPASS/CPMG a powerful technique for rapid acquisition of multidimensional NMR spectra of chalcogenide glasses.

3. Applications of PASS/CPMG and MATPASS/CPMG NMR spectroscopy in Chalcogenide glasses

3.1. Structure of low-dimensional chalcogenides in the system Se-S-Te by ^{77}Se MATPASS NMR

We start this section with the application of ^{77}Se MATPASS/CPMG NMR as a probe for understanding the structure of amorphous Se and of the glasses in the binary elemental systems

Se-S and Se-Te. As mentioned above, the chalcogens S, Se and Te are predominantly twofold coordinated in chalcogenide glasses, which give rise to low-dimensional structural elements such as polymeric chains and rings. While the structures of crystalline S and Te at standard conditions are characterized, respectively, by S_8 rings and $[Te]_n$ polymeric chains, crystalline Se can exist in a stable trigonal and metastable monoclinic forms that consist of helical $[Se]_n$ chains and Se_8 rings, respectively. Therefore, despite its chemical simplicity, the structure of amorphous Se remained quite controversial in the literature with structural models suggesting a coexistence of chain and ring elements [27, 51, 52]. The similarity in the short-range structural aspects between $[Se]_n$ chains and Se_8 rings including the nearest neighbor distances, bond angles, and dihedral angles has made it challenging for diffraction and vibrational spectroscopy to unequivocally distinguish the two types of structural units[51, 52]. In sharp contrast, a recent ^{77}Se MATPASS/CPMG NMR study[27] has shown that the Se nuclides in the chain and ring environments are easily distinguishable based on their δ_{iso}, Δ and η (Fig. 3). The Se chain environment in trigonal Se polymorph is characterized by δ_{iso} = 795 ppm; Δ = –260 ppm and η = 0.7, while these NMR parameters for the 8 different Se sites in a Se_8 ring in monoclinic Se vary within the following ranges: $528 \leq \delta_{iso} \leq 668$ ppm; -450 ppm $\leq \Delta \leq -425$ ppm and $0.2 \leq \eta \leq 0.4$. Amorphous Se displays only one Se environment with NMR parameters δ_{iso} = 850±75 ppm; Δ = –150 ±15 ppm and η = 0.9 ±0.1, which are quite similar to those characteristic of the chain environment in trigonal Se[27]. These results thus, conclusively prove that the structure of amorphous Se consists exclusively of $[Se]_n$ chains.

Further corroboration to this conclusion comes from a structural study of binary S-Se glasses. Glasses can be made continuously between these two elemental endmembers in this binary join [35]. Glasses with high S content display two distinct ^{77}Se isotropic resonances in

the NMR spectrum: one is centered at ~ 850 ppm with $\Delta \approx -153$ ppm and $\eta \approx 0.80$, typical of the -Se-**Se**-Se- environment in $[Se]_n$ chains, while a second resonance at δ_{iso} ~ 640-660 ppm with $\Delta \approx -500$ ppm and $\eta \approx 0.15$ can be readily assigned, on the basis of the discussion above, to Se atoms in a ring environment (Fig. 4). It is well known that the structure of amorphous S consists predominantly of S_8 rings. Therefore, the NMR results suggest that the addition of Se to S results in the replacement of one or more S atoms in these rings. Additionally, the δ_{iso} of the $[Se]_n$ chain environment was found to shift systematically to higher frequencies upon addition of sulfur, which was shown, using density functional theory (DFT) based calculations, to be indicative of incorporation of S atoms into the $[Se]_n$ chains and the consequent formation of -Se-**Se**-S- and -S-**Se**-S- linkages [35]. The compositional variation of the chain vs. ring speciation of Se atoms obtained from the isotropic projection of the MATPASS spectra were shown to be consistent with an average ring composition ranging from Se_1S_7 to $Se_{1.5}S_{6.5}$ (Fig. 5). Therefore, when taken together, these results indicate that the S and Se atoms in binary S_xSe_{100-x} glasses retain their respective preference for forming rings and chains, as in their stable crystalline polymorphs.

As mentioned above, the structure of the stable crystalline polymorphs of Se and Te consists of two-coordinated $[Se]_n$ or $[Te]_n$ helical chains, respectively. However, unlike the S_xSe_{100-x} system, the glass-forming composition range for Te_xSe_{100-x} is significantly limited as Te itself, owing to its high metallicity, is a poor glass-former that can only be vitrified as thin films and readily crystallizes upon supercooling the melt in bulk [34]. Previous MAS NMR studies of Te_xSe_{100-x} glasses utilized experimental conditions that precluded complete separation of spinning sidebands from isotropic peaks due to the relatively large CSA and chemical shift distribution for ^{77}Se (^{125}Te) that are characteristic of the constituent Se (Te) environments[34].

Therefore, the CSA and chemical shift distribution related line broadening was found to be too large to retrieve precise information regarding Se/Te speciation. Below we discuss the application of combined ^{77}Se and

^{125}Te MATPASS/CPMG NMR in a recent study [34] in deciphering the structure of binary Te_xSe_{100-x} glasses with $0 \leq x \leq 35$. It may be noted here that compared to ^{77}Se, ^{125}Te is characterized by significantly larger CSA and chemical shift range and hence, the projection version of the MATPASS pulse sequence *pj*MAT/CPMG was used for covering the wide ^{125}Te frequency range. The isotropic ^{77}Se NMR spectra of these glasses (Fig. 6) show significantly improved resolution compared to the previously published MAS spectra and allow the identification of three partially resolved resonances with δ_{iso} ~ 870, 750 and 600 ppm. The resonances at ~ 750 and 600 ppm appear and grow in intensity with progressive addition of Te to Se. The resonance at ~870 ppm can be unambiguously assigned to Se–**Se**–Se environment, while those at 750 and 600 ppm can be assigned to Se–**Se**–Te and Te–**Se**–Te environments, respectively. The compositional variation of the relative fractions of these Se environments (Fig. 6) shows excellent agreement with a model of random distribution of Se and Te atoms in copolymeric $[Se,Te]_n$ chains with an equal preference for Se (Te) atoms to form Se–Se (Te-Te) and Se–Te bonds. Compared to ^{77}Se, the ^{125}Te isotropic line shapes display lower resolution and signal:noise ratio as the latter are severely broadened by the large ^{125}Te chemical shift distribution (Fig. 7). These ^{125}Te isotropic line shapes were simulated in a consistent fashion by the authors using three resonances centered at δ_{iso} ~ 1100, 1300 and 1500 ppm, corresponding to Te–**Te**–Te, Te–**Te**–Se and Se–**Te**–Se environments, respectively, where they were able to keep the relative areas of the three peaks constrained to those expected for a random distribution [34]. Thus, both ^{77}Se and ^{125}Te NMR spectra were shown to be consistent with a random distribution

of Se and Te atoms in the copolymeric $[Se,Te]_n$ chains in the glass structure. The same study showed that further insights into the bonding environments in these glasses at the next-nearest neighbor level could be obtained from a consideration of the compositional variation of the ^{77}Se CSA parameters [34]. The average Δ for the Se-**Se**-Se sites was shown to decrease systematically from −150 to −170 ppm as δ_{iso} decreased from ~ 880 to 825 ppm, with increasing Te content, which was suggested to be consistent with the replacement of a Se next-nearest neighbor by a Te atom. As discussed in the following section, similar trends were also reported for the Ge-Se system and could be related, with the help of DFT based calculations, to the progressive replacement of Se with Ge as next-nearest neighbors with increasing Ge content.

3.2. ^{77}Se MATPASS NMR spectroscopic study of the structure of Ge_xSe_{1-x} and As_xSe_{1-x} glasses

Binary Ge_xSe_{100-x} glasses have been treated in the literature as model systems for understanding structure-property relationships in complex chalcogenide glasses [7, 10, 11, 22, 53-60]. ^{77}Se MAS NMR was found to be insufficient to average out the CSA-induced spinning sidebands for these glasses. Increased resolution from removal of CSA-induced line broadening could be immediately observed in the isotropic projection of the ^{77}Se MATPASS NMR spectrum of $Ge_{17}Se_{83}$ glass when compared with the MAS spectrum collected at the same ν_r and magnetic field (Figure 8). The compositional evolution of the isotropic NMR spectra for these binary glasses are shown in Figure 9 [7]. Analyses of these line shapes in Figure 9 and of the variation of the CSA as a function of δ_{iso} (Figure 10) allowed for the identification of 4 distinct Se environments with δ_{iso} at ~ 850 (Se-**Se**-Se), 600 (Ge-**Se^{E}**-Ge), 550 (Se-**Se**-Ge) and 400 ppm (Ge-**Se^{C}**-Ge) that are characterized by their unique Δ values. Here the Ge-**Se^{C}**-Ge and Ge-**Se^{E}**-Ge environments correspond to Se sites that belong, respectively, to corner and edge- shared $GeSe_{4/2}$ tetrahedra. The compositional dependence of the relative fraction of Se-**Se**-Se sites in these

glasses could be shown to follow the trend predicted by a stochastic random network model (Fig. 9) where the structural network consists of randomly connected $GeSe_{4/2}$ tetrahedra and Se-Se-Se chain elements.With the success in demonstrating the applicability of ^{77}Se MATPASS NMR for the identification of Se nearest neighbor environments, Kaseman et al. [61] carried out a careful analysis of the compositional variation of the ^{77}Se Δ vs. δ_{iso} for the -Se-**Se**-Se- chain environments in the structure of Ge_xSe_{100-x} glasses. As Figure 11 shows, Δ continually increases across this chemical shift range by 20 ppm, which could be shown using DFT based quantum chemical calculations to be fully consistent with the effect of adding Ge in the NNN position. In fact, a similar, but larger effect is seen in Δ when Ge is added in the NN position. Such analysis enabled the identification and quantitation of three distinct –Se-**Se**-Se- linkages with different number of Ge next-nearest-neighbors (NNN) in Ge_xSe_{100-x} glasses with $5 \leq x \leq 20$ that are: Se-Se-**Se**-Se-Se, Ge-Se-**Se**-Se-Se and Ge-Se-**Se**-Se-Ge [61]. The resulting distribution of Se chains terminated by $GeSe_4$ tetrahedra was shown to closely follow the Flory-Schulz statistics, which was originally developed to describe the chain length distribution for a polymerization process and consistent with the abovementioned stochastic random network model for the short-range order in these glasses. Therefore, such isotropic-anisotropic correlation NMR experiments in combination with DFT-based calculations could be used successfully to investigate the intermediate-range structural order in these chalcogenide glasses at the NNN length scale.

Leveraging the CSA in a correlated dimension proved to be effective in establishing structure-property relationship in As_xSe_{100-x} glasses, where a wide range of physical properties show strongly nonlinear compositional variation [5, 62-64]. The composition dependence of the ^{77}Se MATPASS isotropic projections for these glasses are show in Figure 12. The isotropic projections of Se-rich glasses display 2 resonances with at $\delta_{iso} \sim 850$ and 600 ppm that can be

assigned readily to Se-**Se**-Se and As-**Se**-Se sites. With the addition of 20-40% As, the relative fraction of Se-**Se**-Se chains diminish, while a third resonance at $\delta_{iso} \sim 450$ ppm corresponding to the As-**Se**-As sites begin to appear and rapidly increase in intensity (Fig. 12). At ≥50% As, a resonance at the isotropic position of the Se-**Se**-Se chains reemerges, which at first sight seems anomalous at such high As content. However, an inspection of the CSA at δ_{iso}=850 ppm for isotropic spectra of glasses with 90% and 60% Se shows clear differences with $\Delta \sim -150$ ppm and 800 ppm, respectively (Fig. 13). While $\Delta \sim -150$ ppm is consistent with Se-**Se**-Se chain environment, that of ~ 800 ppm was shown to be related to the appearance of As_4Se_3 molecular units in As_xSe_{100-x} glasses with ≥50% As. The existence of the Se-**Se**-As sites in the most Se-deficient glasses is an intriguing result, which was related on the basis of Raman spectroscopic results to be related to the formation of As-rich clusters and As_4Se_3 molecules with a connective "tissue" that contains the excess Se in these sites.

When taken together, the structural information obtained from the ^{77}Se MATPASS NMR data suggest the presence of 3 different structure types in As_xSe_{100-x} glasses that are fully consistent with the corresponding compositional variation of the physical properties. The composition regions for these three structure types are: (i) that with excess Se (≥ 60at.% Se) where, upon addition of As to Se, the $AsSe_{3/2}$ pyramids progressively crosslink the Se chain environments; (ii) that with 40-50 at. % Se characterized by significant As_4Se_3 molecule formation; and lastly (iii) the As-rich region with <40 at.% Se, characterized by As-rich clusters and As_4Se_3 molecules separated and connected by Se-**Se**-As linkages (Fig. 14). In region (i) increasing cross-linking of the Se chain environments results in a monotonic increase in density ρ and glass transition temperature T_g as well as a monotonic decrease in the coefficient of thermal expansion α. The formation of isolated and van der Waals bonded As_4Se_3 molecular

units in region (ii) lowers the connectivity of the network, which gives rise to a lowering of ρ and T_g and an increase in α. Finally in region (iii) with Se contents <40 at.%, a rapid decrease in the concentration of the As_4Se_3 molecules and the formation of As-rich clusters are consistent with the observed increase in ρ and T_g and decrease in α. These results reveal an intimate connection between the composition dependent variation in the physical properties of As_xSe_{100-x} glasses and their short and intermediate -range structure and bonding.

3.3. ^{29}Si and ^{77}Se MATPASS NMR spectroscopic study of the structure of Si_xSe_{1-x} glasses

The ambient pressure structures of the crystalline and amorphous tetrahedral networks of composition AX_2 in oxides (e.g. SiO_2), halides (e.g. BeF_2) and chalcogenides (e.g. $GeSe_2$) are characterized by either exclusively or predominantly corner-shared $AX_{4/2}$ tetrahedra with a minor fraction of tetrahedra that participate in edge-sharing. In this regard SiX_2 (X=S, Se) is unique as at ambient pressure its crystalline polymorphs are characterized by structures with exclusive or predominant edge-sharing of the constituent tetrahedra [65]. A recent study of a low-temperature crystalline polymorph of $SiSe_2$, using a combination of ^{77}Se and ^{29}Si MAS NMR and DFT calculations of the CSA parameters, has conclusively established the systematics for these nuclides in both corner- and edge- shared tetrahedral environments [65]. The results of this study show that ^{77}Se δ_{iso} and Δ for the corner-shared Si-**Se**-Si site are ~ 200 ppm and 140 ppm, respectively, while those parameters for the edge-shared Si-**Se**-Si sites are significantly larger and range between 280-350 ppm and 250-315 ppm, respectively. On the other hand, the ^{29}Si δ_{iso} and Δ for the doubly edge-shared $SiSe_{4/2}$ tetrahedra (E^2) are significantly different (−85 ppm and 135 ppm, respectively) from those (−63 ppm and −100 ppm, respectively) characteristic of

tetrahedra that share a single edge (E^1). Exclusively corner-shared Si tetrahedra (E^0) are characterized by an even higher δ_{iso} in the range of −30 ppm. However, unlike crystalline polymorphs, glasses in the binary Si_xSe_{1-x} system are characterized by the coexistence of a wide variety of Si and Se species associated with E^0, E^1 and E^2 tetrahedra as well as $SiSe_{4/2}$ tetrahedra cross-linking –Se-Se-Se- chain segments in Se-rich glasses, with each NMR signal being further broadened by structural disorder and CSA (Fig. 15). These issues led Marple et al. [28] to use a combination high-resolution ^{29}Si and ^{77}Se MATPASS NMR spectroscopy and DFT-based calculations to study the composition dependent Si and Se speciation in Si_xSe_{1-x} ($0.05 \leq x \leq 0.33$) glasses.

The ^{29}Si 2D MATPASS NMR spectrum of the Si_xSe_{1-x} glass with x= 0.30 (Fig. 16) demonstrates as a representative for this composition series the unique information content of a two-dimensional isotropic-anisotropic correlation spectrum[28]. This spectrum displays three well-resolved resonances centered at −25, −60, and −90 ppm that are characterized by their distinct Δ and η. Analysis of the anisotropic line shapes indicate that the resonance at −25 ppm has a composite nature consisting of two components at −28 and −17 ppm, which are characterized by positive and negative Δ values (Fig. 16). As discussed above, the resonances centered at −28, −60, and −90 ppm can be readily assigned to Si in E^0, E^1 and E^2 environments, respectively. On the other hand, DFT based calculations by Marple et al. [28] indicated that the resonance at −17 ppm could be assigned to $Se_{3/2}$-**Si**-Se-Se sites, i.e. to $SiSe_{4/2}$ tetrahedra linked to a Se chain segment.

The ^{77}Se MATPASS NMR spectra of these glasses allowed for the identification of two main groups of resonances centered at ~ 850 and 275 ppm, along with a broad and partially

overlapped signal at ~ 650 ppm [28]. The anisotropic line shapes of these resonances yield their characteristic Δ and η parameters, and when taken together with δ_{iso}, the resonances at ~ 850, 650 and 275 ppm could be assigned to Se-**Se**-Se, Si-**Se**-Se and Si-**Se**-Si sites, respectively. Furthermore, the isotropic ^{77}Se NMR spectra of glasses near the stoichiometric (x=0.33) composition revealed the presence of two broad resonances centered at ~ 325 and 225 ppm (Fig. 17), which could be assigned on the basis of the NMR results obtained on the low-temperature polymorph of $SiSe_2$, to Se sites of the type E^1-**Se**-E^1 and E^2-**Se**-E^1/E^2, respectively. The compositional evolution of the relative fractions of these Se environments, as obtained from the ^{77}Se MATPASS NMR spectra, indicated the progressive replacement of Se chains with corner- and edge- sharing $SiSe_4$ tetrahedra in the structure of Si_xSe_{1-x} glasses with increasing x. However, unlike ^{29}Si, the ^{77}Se MATPASS spectra of the Si_xSe_{1-x} glasses were found to be non-quantitative as different resonances in the spectra were characterized by different spin-lattice relaxation rates and fully relaxed spectra could not be collected due to time constraints. Therefore, the compositional variation of the relative fractions of the four Si environments, as obtained from the ^{29}Si MATPASS NMR spectra, was used by Marple et al. [28] to test three distinct structural scenarios for these glasses: the chain-crossing model, the cluster model and the stochastic random network (SRN) model. The chain-crossing model is based on the perfect avoidance and maximum separation of the $SiSe_{4/2}$ tetrahedra, while the clustering model corresponds to a complete separation of the Se chain and $SiSe_{4/2}$ tetrahedral environments such that all $SiSe_{4/2}$ tetrahedra are connected via corner- and edge–sharing. In contrast, the SRN model is characterized by random connectivity between the $SiSe_{4/2}$ tetrahedra and the Se-Se chain elements. Marple et al.'s analysis indicated that the structure of Si_xSe_{1-x} glasses could be best described using the cluster model where the network is formed by randomly interconnected

small nanoclusters of E^0, E^1 and E^2 tetrahedra interconnected via Si-Se-Se linkages [28]. These clusters coalesce near $x \geq 0.2$, and ultimately form a low-dimensional network consisting of short chains of edge-sharing tetrahedra cross-linked by corner-shared tetrahedra at the stoichiometric composition ($x=0.33$).

3.4. ^{31}P PASS NMR spectroscopic study of the rotational dynamics in a molecular glass

While structural characterizations have been highlighted throughout this manuscript, we end this review with an application of ^{31}P isotropic-anisotropic correlation spectroscopy using the PASS experiment to study the rotational dynamics of the constituent P_4Se_3 molecules in a P-Se glass-forming liquid of composition P_5Se_3 [37]. The P_4Se_3 cage like molecules, which are held together via Van der Waals forces, result in a low T_g (298 K) for this glass. The ^{31}P PASS experiment was carried out at a low spinning speed (3 kHz), which resulted in a sideband pattern for the apical and basal P atoms in the molecule that closely mirrored the static powder pattern (Fig. 18). The rotational motion of these molecules was shown to result in dynamic averaging of the ^{31}P CSA (Fig. 19), which was successfully simulated using a model of isotropic rotational reorientation to extract the timescale of the dynamics τ_R at different temperatures [37]. This timescale showed a nearly-Arrhenius temperature dependence with anomalously large decoupling from the shear relaxation timescale τ_M of the liquid i.e. $\tau_R << \tau_M$ (Fig. 20). This behavior, along with the behavior observed in As_4S_3 glass [66], is in sharp contrast with those reported in previous studies on organic molecular glass-forming liquids [67-69], which indicated that the average rotational correlation times of the constituent molecules are strongly coupled to the shear and structural relaxation time scales at all temperatures above T_g.

4. Conclusions and Future Directions

This review demonstrates that in spite of the challenges associated with high-resolution solid-state NMR spectroscopy of chalcogenide glasses, the utilization of the MATPASS/CPMG isotropic-anisotropic correlation spectroscopy has provided a tremendous wealth of information on the short- and intermediate- range structural attributes in a wide variety of chalcogenide glass

systems to date. As noted in the previous sections, application of such spectroscopic technique can be even more powerful in combination with DFT computations of the chemical shift tensor for various structural moieties. This approach allowed for the identification of molecular units in As-Se glasses, the quantitation of chain length statistics and next-nearest-neighbor environments in Ge-Se glasses and conclusive distinction of Se in ring vs. chain environments in S-Se glasses. We anticipate such combined use of DFT and isotropic-anisotropic correlation NMR in the future in addressing a wider variety of structural problems including the determination of bond angle distributions, bond length vs. bond angle correlations, inter-chain vs. intra-chain correlations in chalcogenide glasses.

Sensitivity is always going to be an issue with NMR spectroscopy on chalcogenide glasses in general, due to the low natural abundances and long spin-lattice relaxation times of many of the constituent nuclei. While this issue is partially addressed with the incorporation of CPMG echo-train acquisition, additional sensitivity may be gained, especially for 2D experiments, using cross-polarization (CP) techniques. The efficacy of polarization transfer from ^{31}P to ^{77}Se nuclides via ^{31}P$\rightarrow$^{77}Se CP has been previously demonstrated in P-Se glasses, which led to enhanced ^{77}Se signals [70]. However, majority of chalcogenide systems do not contain spin-1/2 nuclides with high gyromagnetic ratio γ in high enough abundance for routine employment of CP. Although it requires specialized instrumentation, another polarization transfer technique known as dynamic nuclear polarization (DNP) is an attractive alternative to CP, which employs polarization transfer from unpaired electron spins in the system. Such unpaired electrons can be introduced into the system via creation of stable radicals using e.g. γ-radiation or via purposeful doping with transition metals or rare earth ions into the matrix [71, 72]. We expect that in future applications of NMR spectroscopy in chalcogenides, CP or DNP

will be used in conjunction with CPMG to provide a means for maximizing the signal to enable a wide variety of 2D experiments.

Acknowledgement

This work was supported by a grant from the National Science Foundation (NSF-DMR 1855176) to SS. The high-field MATPASS/CPMG NMR spectra for all the work reviewed here were collected at the National High Magnetic Field Laboratory (NHMFL) in Tallahassee, FL, USA, which was supported through NSF DMR-1157490 and DMR-1644779 and the State of Florida. SS also acknowledges his long-standing collaboration with Dr. Zhehong Gan and Dr. Ivan Hung at the NHMFL on matters both experimental and theoretical, associated with MATPASS/CPMG NMR. This work is released for publication in accordance with Los Alamos National Laboratory LA-UR-20-26008 by Triad National Security, LLC (Los Alamos, NM, USA) operator of the Los Alamos National Laboratory under contract no. 89233218CNA000001 with the U.S. Department of Energy.

References

[1] A. Hilton, Chalcogenide glasses for infrared optics, McGraw-Hill, Inc., 2010.
[2] B. Bureau, X.H. Zhang, F. Smektala, J.-L. Adam, J. Troles, H.-l. Ma, C. Boussard-Plèdel, J. Lucas, P. Lucas, D. Le Coq, M.R. Riley, J.H. Simmons, Recent advances in chalcogenide glasses, J. Non-Cryst. Solids, 345-346 (2004) 276-283.
[3] M. Wuttig, N. Yamada, Phase-change materials for rewriteable data storage, Nat. Mater., 6 (2007) 824-832.
[4] A. Zakery, S.R. Elliott, Optical properties and applications of chalcogenide glasses: a review, J. Non-Cryst. Solids, 330 (2003) 1-12.
[5] D.C. Kaseman, I. Hung, Z. Gan, B. Aitken, S. Currie, S. Sen, Structural and Topological Control on Physical Properties of Arsenic Selenide Glasses, J. Phys. Chem. B, 118 (2014) 2284-2293.
[6] G. Yang, B. Bureau, T. Rouxel, Y. Gueguen, O. Gulbiten, C. Roiland, E. Soignard, J.L. Yarger, J. Troles, J.-C. Sangleboeuf, P. Lucas, Correlation between structure and physical properties of chalcogenide glasses in the AsxSe1-x system, Physical Review B, 82 (2010) 195206.
[7] D.C. Kaseman, I. Hung, Z. Gan, S. Sen, Observation of a Continuous Random Network Structure in GexSe100–x Glasses: Results from High-Resolution 77Se MATPASS/CPMG NMR Spectroscopy, J. Phys. Chem. B, 117 (2013) 949-954.
[8] S. Soyer Uzun, S. Sen, C.J. Benmore, B.G. Aitken, A combined neutron and x-ray diffraction study of short- and intermediate-range structural characteristics of Ge–As sulfide glasses, J. Phys.: Condens. Matter, 20 (2008) 335105.
[9] S. Soyer-Uzun, S. Sen, B.G. Aitken, Network vs Molecular Structural Characteristics of Ge-Doped Arsenic Sulfide Glasses: A Combined Neutron/X-ray Diffraction, Extended X-ray Absorption Fine Structure, and Raman Spectroscopic Study, J. Phys. Chem. C, 113 (2009) 6231-6242.
[10] E.L. Gjersing, S. Sen, B.G. Aitken, Structure, Connectivity, and Configurational Entropy of GexSe100−x Glasses: Results from 77Se MAS NMR Spectroscopy, J. Phys. Chem. C, 114 (2010) 8601-8608.
[11] T.G. Edwards, S. Sen, E.L. Gjersing, A combined 77Se NMR and Raman spectroscopic study of the structure of GexSe1-x glasses: Towards a self consistent structural model, J. Non-Cryst. Solids, 358 (2012) 609-614.
[12] E.L. Gjersing, S. Sen, B.G. Aitken, Molecular Dynamics in Supercooled P−Se Liquids near the Glass Transition: Results from 31P NMR Spectroscopy, J. Phys. Chem. B, 115 (2011) 2857-2863.
[13] B. Kalkan, C.J. Benmore, B.G. Aitken, S. Sen, S.M. Clark, A comparative study of the atomic structures of Ge-doped As4S3 and P4Se3 molecular glasses, J. Non-Cryst. Solids, 514 (2019) 83-89.
[14] J. Herzfeld, A.E. Berger, Sideband intensities in NMR spectra of samples spinning at the magic angle, J. Chem. Phys., 73 (1980) 6021-6030.
[15] A. Bytchkov, F. Fayon, D. Massiot, L. Hennet, D.L. Price, 31P solid-state NMR studies of the short-range order in phosphorus–selenium glasses, Phys. Chem. Chem. Phys., 12 (2010) 1535-1542.

[16] D.C. Kaseman, I. Hung, K. Lee, K. Kovnir, Z. Gan, B. Aitken, S. Sen, Tellurium Speciation, Connectivity, and Chemical Order in AsxTe100–x Glasses: Results from Two-Dimensional 125Te NMR Spectroscopy, J. Phys. Chem. B, 119 (2015) 2081-2088.
[17] T.G. Edwards, E.L. Gjersing, S. Sen, S.C. Currie, B.G. Aitken, 125Te NMR chemical shifts and tellurium coordination environments in crystals and glasses in the Ge–As–Sb–Te system, J. Non-Cryst. Solids, 357 (2011) 3036-3041.
[18] S. Sen, Z. Gan, Chemical order around Ge atoms in binary germanium selenide glasses: Results from 73Ge solid-state NMR spectroscopy at 19.6 Tesla, J. Non-Cryst. Solids, 356 (2010) 1519-1521.
[19] R. Maxwell, D. Lathrop, H. Eckert, Intermediate-range order in phosphorus-selenium glasses. Constraints from 31P and 77Se NMR spectroscopy, J. Non-Cryst. Solids, 180 (1995) 244-250.
[20] D. Lathrop, H. Eckert, Dipolar NMR spectroscopy of nonoxidic glasses. Structural characterization of the system phosphorus-selenium by phosphorus-31-selenium-77 spin echo double resonance NMR, J. Am. Chem. Soc., 112 (1990) 9017-9019.
[21] R. Maxwell, H. Eckert, Chemical equilibria in glass-forming melts: high-temperature 31P and 77Se NMR of the phosphorus-selenium system, J. Am. Chem. Soc., 116 (1994) 682-689.
[22] B. Bureau, J. Troles, M. Le Floch, P. Guénot, F. Smektala, J. Lucas, Germanium selenide glass structures studied by 77Se solid state NMR and mass spectroscopy, J. Non-Cryst. Solids, 319 (2003) 145-153.
[23] B. Bureau, J. Troles, M. LeFloch, F. Smektala, G. Silly, J. Lucas, Solid state 77Se NMR investigations on arsenic-selenium glasses and crystals, Solid State Sci., 5 (2003) 219-224.
[24] P.C. Taylor, P. Hari, A. Kleinhammes, P.L. Kuhns, W.G. Moulton, N.S. Sullivan, Asymmetries in local bonding sites in amorphous semiconductors: very high field NMR of 75As, J. Non-Cryst. Solids, 227-230 (1998) 770-774.
[25] P.C. Taylor, T. Su, P. Hari, E. Ahn, A. Kleinhammes, P.L. Kuhns, W.G. Moulton, N.S. Sullivan, Structural and photostructural properties of chalcogenide glasses: recent results from magnetic resonance measurements, J. Non-Cryst. Solids, 326-327 (2003) 193-198.
[26] I. Hung, T. Edwards, S. Sen, Z. Gan, MATPASS/CPMG: A sensitivity enhanced magic-angle spinning sideband separation experiment for disordered solids, J. Magn. Reson., 221 (2012) 103-109.
[27] M. Marple, J. Badger, I. Hung, Z. Gan, K. Kovnir, S. Sen, Structure of Amorphous Selenium by 2D 77Se NMR Spectroscopy: An End to the Dilemma of Chain versus Ring, Angew. Chem. Int. Ed., 56 (2017) 9777-9781.
[28] M.A.T. Marple, I. Hung, Z. Gan, S. Sen, Structural and Topological Evolution in SixSe1–x Glasses: Results from 1D and 2D 29Si and 77Se NMR Spectroscopy, J. Phys. Chem. B, 121 (2017) 4283-4292.
[29] M.A.T. Marple, I. Hung, Z. Gan, S. Sen, Structural and Topological Evolution in SixSe1-x, Glasses: Results from 1D and 2D Si-29 and Se-77 NMR Spectroscopy, J. Phys. Chem. B, 121 (2017) 4283-4292.
[30] M.A.T. Marple, M. Jesuit, I. Hung, Z. Gan, S. Feller, S. Sen, Structure of TeO2 glass: Results from 2D Te-125 NMR spectroscopy, J. Non-Cryst. Solids, 513 (2019) 183-190.
[31] M.A.T. Marple, D.C. Kaseman, I. Hung, Z. Gan, S. Sen, Structure and physical properties of glasses in the system Ag2Se-Ga2Se3-GeSe2, J. Non-Cryst. Solids, 437 (2016) 34-42.
[32] Z. Whittles, M. Marple, I. Hung, Z. Gan, S. Sen, Structure of BaO-TeO2 glasses: A two-dimensional Te-125 NMR spectroscopic study, J. Non-Cryst. Solids, 481 (2018) 282-288.

[33] Y. Xia, M.A.T. Marple, I. Hung, Z. Gan, S. Sen, Network Structure and Connectivity in SnO-P2O5 Glasses: Results from 2D P-31 and Sn-119 NMR Spectroscopy, JPCB, 122 (2018) 7416-7425.
[34] B. Yuan, I. Hung, Z. Gan, S. Sen, Chemical order in binary Se-Te glasses: Results from high-resolution 2D 77Se and 125Te MATPASS NMR spectroscopy, J. Non-Cryst. Solids, 544 (2020) 120212.
[35] B. Yuan, W. Zhu, I. Hung, Z. Gan, B. Aitken, S. Sen, Structure and Chemical Order in S–Se Binary Glasses, J. Phys. Chem. B, 122 (2018) 12219-12226.
[36] D.C. Kaseman, T. Endo, S. Sen, Structural disorder and the effects of aging in a phosphate glass: Results from two-dimensional 31P PASS NMR spectroscopy, J. Non-Cryst. Solids, 359 (2013) 33-39.
[37] D.C. Kaseman, O. Gulbiten, B.G. Aitken, S. Sen, Isotropic rotation vs. shear relaxation in supercooled liquids with globular cage molecules, J. Chem. Phys., 144 (2016) 174501.
[38] J.H. Baltisberger, P. Florian, E.G. Keeler, P.A. Phyo, K.J. Sanders, P.J. Grandinetti, Modifier cation effects on 29Si nuclear shielding anisotropies in silicate glasses, J. Magn. Reson., 268 (2016) 95-106.
[39] M.C. Davis, D.C. Kaseman, S.M. Parvani, K.J. Sanders, P.J. Grandinetti, D. Massiot, P. Florian, Q(n) Species Distribution in K2O·2SiO2 Glass by 29Si Magic Angle Flipping NMR, J. Phys. Chem. A, 114 (2010) 5503-5508.
[40] M.C. Davis, K.J. Sanders, P.J. Grandinetti, S.J. Gaudio, S. Sen, Structural investigations of magnesium silicate glasses by 29Si 2D Magic-Angle Flipping NMR, J. Non-Cryst. Solids, 357 (2011) 2787-2795.
[41] B.J. Walder, K.K. Dey, D.C. Kaseman, J.H. Baltisberger, P.J. Grandinetti, Sideband separation experiments in NMR with phase incremented echo train acquisition, J. Chem. Phys., 138 (2013) 174203.
[42] F. Fayon, C. Bessada, A. Douy, D. Massiot, Chemical Bonding of Lead in Glasses through Isotropic vs Anisotropic Correlation: PASS Shifted Echo, J. Magn. Reson., 137 (1999) 116-121.
[43] W.T. Dixon, Spinning-Sideband-Free NMR-Spectra, J. Magn. Reson., 44 (1981) 220-223.
[44] W.T. Dixon, Spinning-Sideband-Free and Spinning-Sideband-Only NMR-Spectra in Spinning Samples, JChPh, 77 (1982) 1800-1809.
[45] O.N. Antzutkin, S.C. Shekar, M.H. Levitt, Two-Dimensional Sideband Separation in Magic-Angle-Spinning NMR, J. Magn. Reson., 115 (1995) 7-19.
[46] Z. Gan, High-resolution chemical shift and chemical shift anisotropy correlation in solids using slow magic angle spinning, J. Am. Chem. Soc., 114 (1992) 8307-8309.
[47] J.Z. Hu, D.W. Alderman, C.H. Ye, R.J. Pugmire, D.M. Grant, An Isotropic Chemical Shift-Chemical Shift Anisotropy Magic-Angle Slow-Spinning 2D NMR Experiment, J. Magn. Reson., 105 (1993) 82-87.
[48] I. Hung, Z. Gan, On the magic-angle turning and phase-adjusted spinning sidebands experiments, J. Magn. Reson., 204 (2010) 150-154.
[49] H.Y. Carr, E.M. Purcell, Effects of Diffusion on Free Precession in Nuclear Magnetic Resonance Experiments, Phys. Rev., 94 (1954) 630-638.
[50] S. Meiboom, D. Gill, Modified Spin- Echo Method for Measuring Nuclear Relaxation Times, Rev. Sci. Instrum., 29 (1958) 688-691.
[51] R.M. Martin, G. Lucovsky, K. Helliwell, Intermolecular bonding and lattice dynamics of Se and Te, Phys. Rev. B, 13 (1976) 1383-1395.

[52] R. Brüning, E. Irving, G. LeBlanc, Reverse Monte Carlo study of structural relaxation in vitreous selenium, J. Appl. Phys., 89 (2001) 3215-3222.
[53] P. Boolchand, X. Feng, W.J. Bresser, Rigidity transitions in binary Ge–Se glasses and the intermediate phase, J. Non-Cryst. Solids, 293-295 (2001) 348-356.
[54] J.C. Phillips, Topology of covalent non-crystalline solids I: Short-range order in chalcogenide alloys, J. Non-Cryst. Solids, 34 (1979) 153-181.
[55] M.F. Thorpe, Continuous deformations in random networks, J. Non-Cryst. Solids, 57 (1983) 355-370.
[56] B. Bureau, J. Troles, M. Le Floch, F. Smektala, J. Lucas, Medium range order studied in selenide glasses by 77Se NMR, J. Non-Cryst. Solids, 326-327 (2003) 58-63.
[57] G. Lucovsky, F.L. Galeener, R.C. Keezer, R.H. Geils, H.A. Six, Structural interpretation of the infrared and Raman spectra of glasses in the alloy system Ge1-xSx, Phys. Rev. B, 10 (1974) 5134-5146.
[58] P. Lucas, E.A. King, O. Gulbiten, J.L. Yarger, E. Soignard, B. Bureau, Bimodal phase percolation model for the structure of Ge-Se glasses and the existence of the intermediate phase, Phys. Rev. B, 80 (2009) 214114.
[59] P. Tronc, M. Bensoussan, A. Brenac, C. Sebenne, Optical-Absorption Edge and Raman Scattering in GexSe1-x Glasses, Phys. Rev. B, 8 (1973) 5947-5956.
[60] E.L. Gjersing, S. Sen, R.E. Youngman, Mechanistic understanding of the effect of rigidity percolation on structural relaxation in supercooled germanium selenide liquids, Phys. Rev. B, 82 (2010) 014203.
[61] D.C. Kaseman, K.M. Oliveira, T. Palazzo, S. Sen, Selenium Chain Length Distribution in GexSe100–x Glasses: Insights from 77Se NMR Spectroscopy and Quantum Chemical Calculations, J. Phys. Chem. B, 120 (2016) 4513-4521.
[62] G. Yang, B. Bureau, T. Rouxel, Y. Gueguen, O. Gulbiten, C. Roiland, E. Soignard, J.L. Yarger, J. Troles, J.-C. Sangleboeuf, P. Lucas, Correlation between structure and physical properties of chalcogenide glasses in the AsxSe1-x system, Phys. Rev. B, 82 (2010) 195206.
[63] G. Yang, O. Gulbiten, Y. Gueguen, B. Bureau, J.-C. Sangleboeuf, C. Roiland, E.A. King, P. Lucas, Fragile-strong behavior in the AsxSe1-x glass forming system in relation to structural dimensionality, Phys. Rev. B, 85 (2012) 144107.
[64] J.D. Musgraves, P. Wachtel, S. Novak, J. Wilkinson, K. Richardson, Composition dependence of the viscosity and other physical properties in the arsenic selenide glass system, J. Appl. Phys., 110 (2011) 063503.
[65] J. Wang, M. Marple, K. Lee, S. Sen, K. Kovnir, Synthesis, crystal structure, and advanced NMR characterization of a low temperature polymorph of SiSe2, J. Mater. Chem. A, 4 (2016) 11276-11283.
[66] E.L. Gjersing, S. Sen, P. Yu, B.G. Aitken, Anomalously large decoupling of rotational and shear relaxation in a molecular glass, Phys. Rev. B, 76 (2007) 214202.
[67] F. Fujara, B. Geil, H. Sillescu, G. Fleischer, Translational and rotational diffusion in supercooled orthoterphenyl close to the glass transition, ZPhyB, 88 (1992) 195-204.
[68] P.G. Debenedetti, F.H. Stillinger, Supercooled liquids and the glass transition, Nature, 410 (2001) 259-267.
[69] M.D. Ediger, Spatially Heterogeneous Dynamics in Supercooled Liquids, ARPC, 51 (2000) 99-128.
[70] T. Pietraβ, R. Seydoux, R.E. Roth, H. Eckert, A. Pines, 31P to 77Se cross polarization in β-P4Se3, Solid State Nucl. Magn. Reson., 8 (1997) 265-267.

[71] S.L. Carnahan, A. Venkatesh, F.A. Perras, J.F. Wishart, A.J. Rossini, High-Field Magic Angle Spinning Dynamic Nuclear Polarization Using Radicals Created by γ-Irradiation, J. Phys. Chem. Lett, 10 (2019) 4770-4776.
[72] A. Harchol, G. Reuveni, V. Ri, B. Thomas, R. Carmieli, R.H. Herber, C. Kim, M. Leskes, Endogenous Dynamic Nuclear Polarization for Sensitivity Enhancement in Solid-State NMR of Electrode Materials, J. Phys. Chem. C, 124 (2020) 7082-7090.

Figure Captions:

Figure 1. Evolution of structural moieties and connectivity in binary glasses. The molecular As_4Se_3 units coexist with network elements in high-As glasses (see section 3.2 for details).

Figure 2. Pulse sequences for (a) PASS and (b) MAT experiments. Both sequences have a $\pi/2$ pulse followed by a train of five π pulses. The time between π pulses is varied in the 2D experiments as shown by the solid blue and black lines perpendicular to the pulses. Note that for MAT the timings are varied in a linear manner, while the PASS timings are not. The timings are relative to the $\pi/2$ pulse, but must be an integer multiple (b) of the rotor period (τ_r). Figure is reproduced from [48] with permission.

Figure 3. 2D ^{77}Se MATPASS spectra of amorphous Se (top) and of Se_8 ring environments in crystalline monoclinic Se (bottom). The bottom panel also shows the spectrum of Se chain environment in trigonal selenium (*t-Se*), which exist as an "impurity phase" in the sample. Note the difference in the anisotropic scale between the top and bottom panels. Figure is reproduced from [27] with permission.

Figure 4. 2D ^{77}Se MATPASS spectrum of $S_{75}Se_{25}$ glass and its total isotropic projection showing signal from Se in chain (left peak) and ring (right peak) environments. Figure is reproduced from [35] with permission.

Figure 5. Left: Compositional evolution of the isotropic ^{77}Se spectra of binary S-Se glasses. Glass compositions are given alongside the spectra. Right: Relative fraction of Se in chains (squares) and rings (circles) as a function of S content, in binary S-Se glasses. Dashed (dotted) orange and blue lines are expected Se site fractions in chains and rings, respectively, for an average 8-membered ring composition of Se_1S_7 ($Se_{1.5}S_{6.5}$) in these glasses. Figure is reproduced from [35] with permission.

Figure 6. Left: Variation of (a) Se–**Se**–Se, (b) Te–**Se**–Se and (c) Te–**Se**–Te site fractions (black squares) as a function of Te content in Te_xSe_{100-x} glasses, derived from simulations of ^{77}Se isotropic NMR spectra on the right. Literature values from a previous ^{77}Se MAS NMR spectroscopic study (purple triangles), chain crossing model (dashed black line), random distribution model (solid red line), and partially random distribution model with some preference for heteropolar bonding (dashed dotted black line). Right: Experimental (black solid lines) and

simulated (red dashed lines) ^{77}Se isotropic NMR spectra for Te_xSe_{100-x} glasses. Individual simulation components for Se–**Se**–Se, Te–**Se**–Se and Te–**Se**–Te sites are shown in blue, green and pink, respectively. Figure is reproduced from [34] with permission.

Figure 7. Experimental (black solid lines) and simulated (orange dashed lines) ^{125}Te isotropic NMR spectra for Te_xSe_{100-x} glasses. Individual simulation components for Se–**Te**–Se, Te–**Te**–Se and Te–**Te**–Te environments are shown in blue, green and pink, respectively. Figure is reproduced from [34] with permission.

Figure 8. 2D ^{77}Se MATPASS/CPMG spectrum of $Ge_{17}Se_{83}$ glass after data processing (bottom). The isotropic projection (blue), is clearly more resolved than the MAS spectrum collected at the same spinning speed (green). Figure is reproduced from [7] with permission.

Figure 9. (a) ^{77}Se isotropic NMR spectra of Ge_xSe_{100-x} glasses showing average chemical shifts for various Se environments. (b) Simulation of the isotropic spectra provides the relative fraction of Se-**Se**-Se sites (black squares), which is compared to the expected values from chain crossing model (blue triangles), clustering model (red circles), and stochastic random network model (green triangles). Figure is reproduced from [7] with permission.

Figure 10. Experimental CSA sideband patterns (black) for the 4 Se environments in Ge_xSe_{100-x} glasses. The CSA parameters are listed for each environment and were obtained by simulation (red) of the experimental spectra. Figure is reproduced from [7] with permission.

Figure 11. Dependence of the Se-**Se**-Se Δ as a function of δ_{iso} for a variety of Ge_xSe_{100-x} glasses. As the chemical shift decreases, the effect of having a Ge atom in a NNN position increases Δ, eventually reaching a plateau as the Se NNN contributions diminish to a negligible fraction of δ_{iso}. The reduction in Se NNN occurs as both a function of δ_{iso} and the glass composition. Figure is reproduced from [61] with permission.

Figure 12. Evolution of the 77Se isotropic NMR spectra of As_xSe_{100-x} glasses showing average chemical shifts for various Se environments. The experimental spectrum is denoted by the black line and the simulated spectrum is given by the red line. Individual simulation components are shown in blue (Se-**Se**-Se environments), red (As-**Se**-Se), green (As-**Se**-As), and orange (As-**Se**-As environments in As_4Se_3 molecular units). Figure is reproduced from [5] with permission.

Figure 13. CSA sideband patterns for the different Se environments in As_xSe_{100-x} glasses. Figure is reproduced from [5] with permission.

Figure 14. Schematic of the structural evolution in As_xSe_{100-x} glasses with composition. As and Se atoms are shown in green and red, respectively. See text for details. Figure is reproduced from [5] with permission.

Figure 15. Various structural moieties in Si_xSe_{1-x} glasses. Figure is reproduced from [28] with permission.

Figure 16. 2D ^{29}Si MATPASS NMR spectrum of $Si_{0.3}Se_{0.7}$ glass. The total isotropic projection is shown with blue solid line. The experimental (black lines) and simulated (red lines) sideband spike patterns (black lines) in the aniostropic dimension for the $(Se)_{3/2}$-**Si**-Se-Se, E^0, E^1 and E^2 environments are also shown. Figure is reproduced from [28] with permission.

Figure 17. ^{77}Se MATPASS NMR spectra of (left) $Si_{0.33}Se_{0.67}$ and (right) $Si_{0.20}Se_{0.80}$ glasses. The total projection on the isotropic dimension for each spectrum is shown with blue solid line. The broad resonances centered at ~ 325 and 225 ppm in the spectrum of $Si_{0.33}Se_{0.67}$ glass correspond to E^1-**Se**-E^1 and E^2-**Se**-E^1/E^2 sites respectively. Peaks in the spectrum of $Si_{0.20}Se_{0.80}$ glass at ~ 850 and 275 ppm correspond to Se-**Se**-Se and Si-**Se**-Si sites, respectively. Figure is reproduced from [28] with permission.

Figure 18. 2D ^{31}P PASS spectrum of P_5Se_3 glass. This glass consists of P_4Se_3 cage-like molecules, in which the P atoms (orange) occupy the apical and basal positions. Se atoms are shown in pink. The isotropic projection is shown above the 2D plot, while the low temperature CSA projections for the apical and basal sites are shown to the right, clearly indicating difference CSA parameters between the environments. Figure is reproduced from [37] with permission.

Figure 19. The averaging of the CSA for the apical sites (left) and basal sites (right) becomes evident as the temperature is increased from 253K to 338K resulting in fewer observable sidebands. Figure is reproduced from [37] with permission.

Figure 20. Comparison between the temperature dependences of τ_R (triangles) as obtained from ^{31}P NMR line shape simulations and that of τ_M (solid line) for supercooled P_5Se_3 liquid. Red circles correspond to τ_M obtained from viscosity measurements. The τ_R (squares) and τ_M (dashed

line) for the P-doped $Ge_3As_{52}S_{45}$ liquid, consisting of similar PAs_3S_3 cage molecules as reported in a previous study [65], are shown for comparison. Figure is reproduced from [37] with permission.

Figure 1

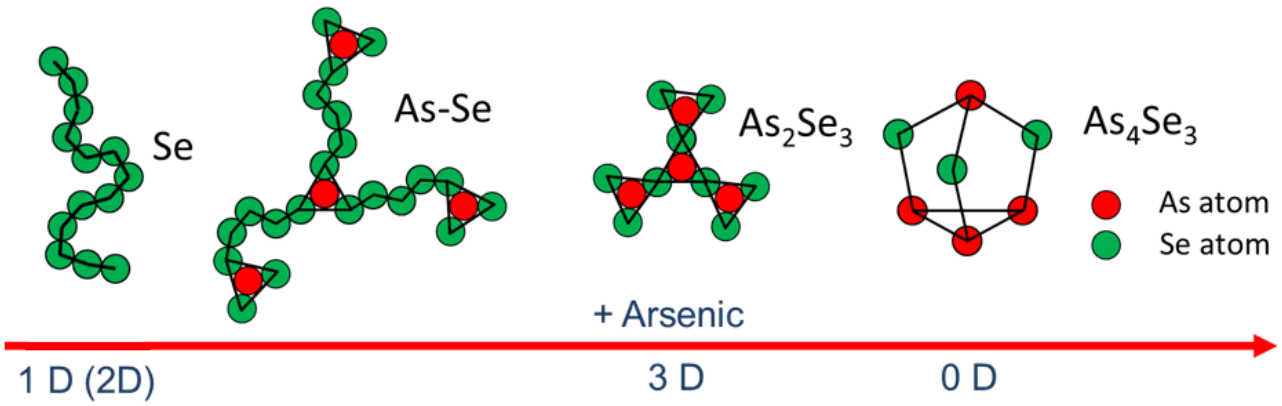

Figure 2

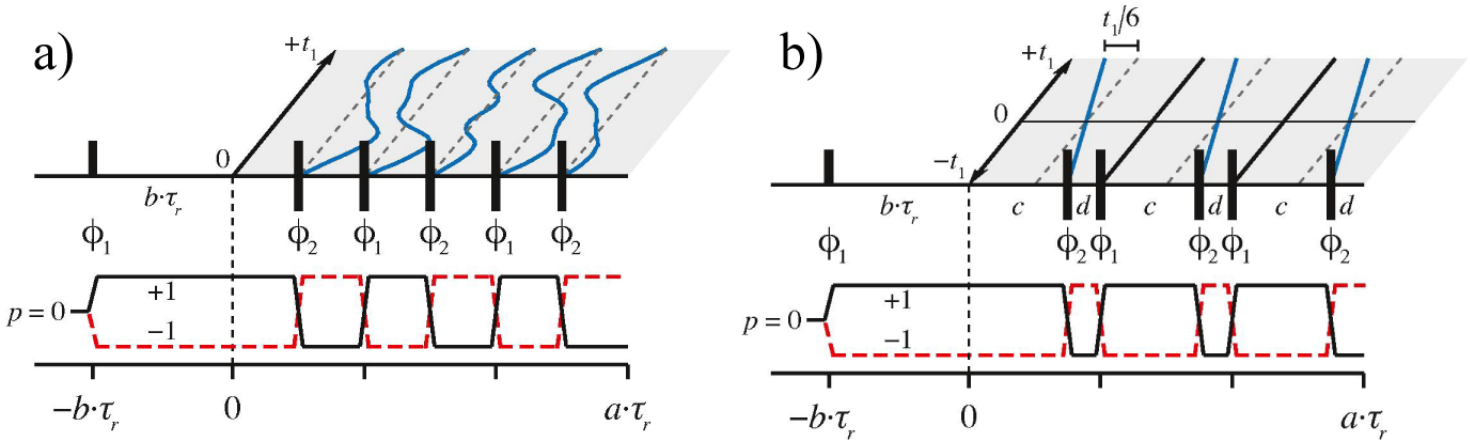
a)
+t1
0
b·τr
Φ1
Φ2 Φ1 Φ2 Φ1 Φ2
p = 0
+1
−1
−b·τr
0
a·τr
b)
t1/6
+t1
0
−t1
b·τr
c d c d c d
Φ1
Φ2 Φ1 Φ2 Φ1 Φ2
p = 0
+1
−1
−b·τr
0
a·τr

Figure 3

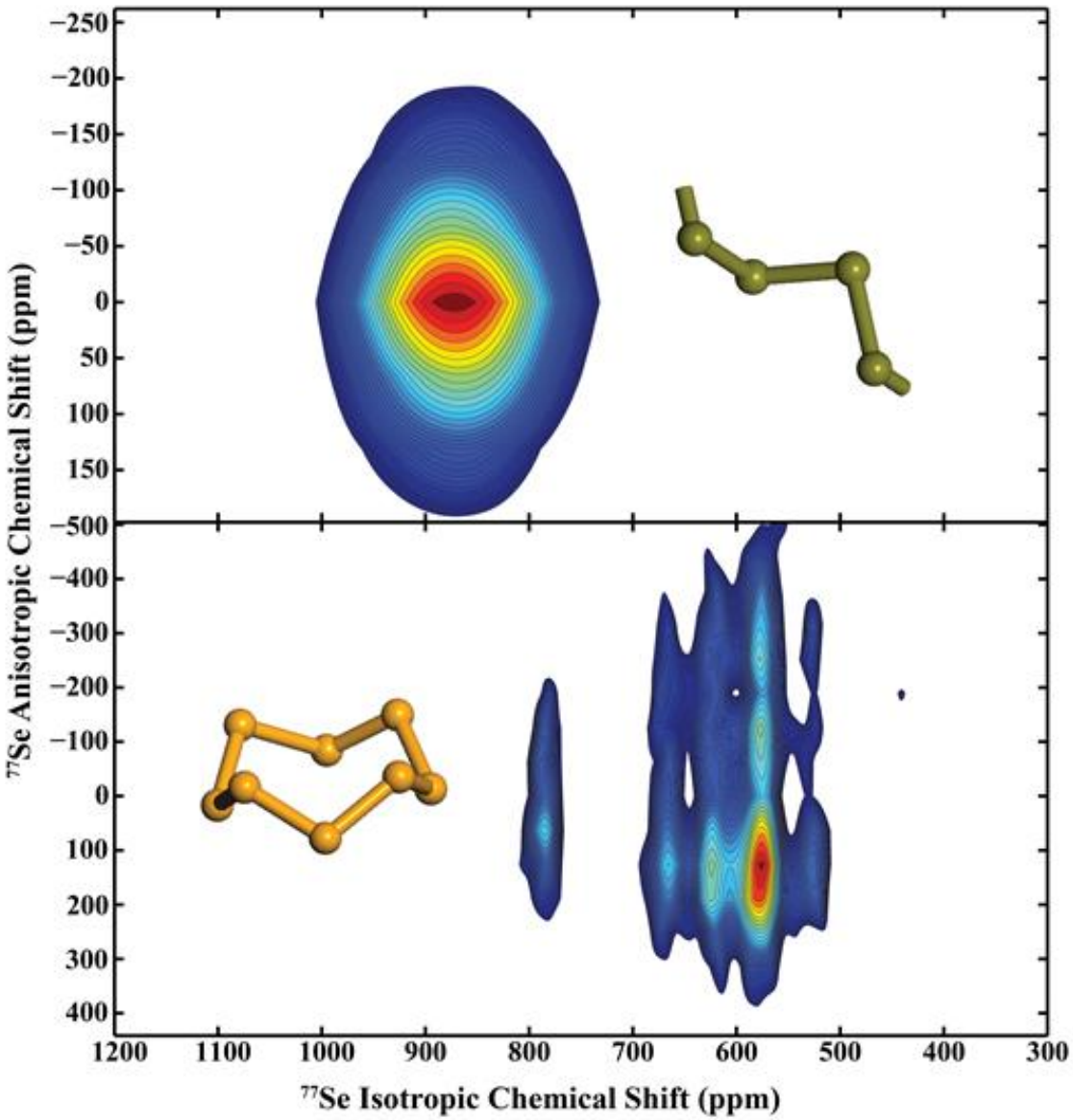
−250
−200
−150
−100
−50
0
50
100
150
−500
−400
−300
−200
−100
0
100
200
300
400
1200
1100
1000
900
800
700
600
500
400
300
77Se Anisotropic Chemical Shift (ppm)
77Se Isotropic Chemical Shift (ppm)

Figure 4

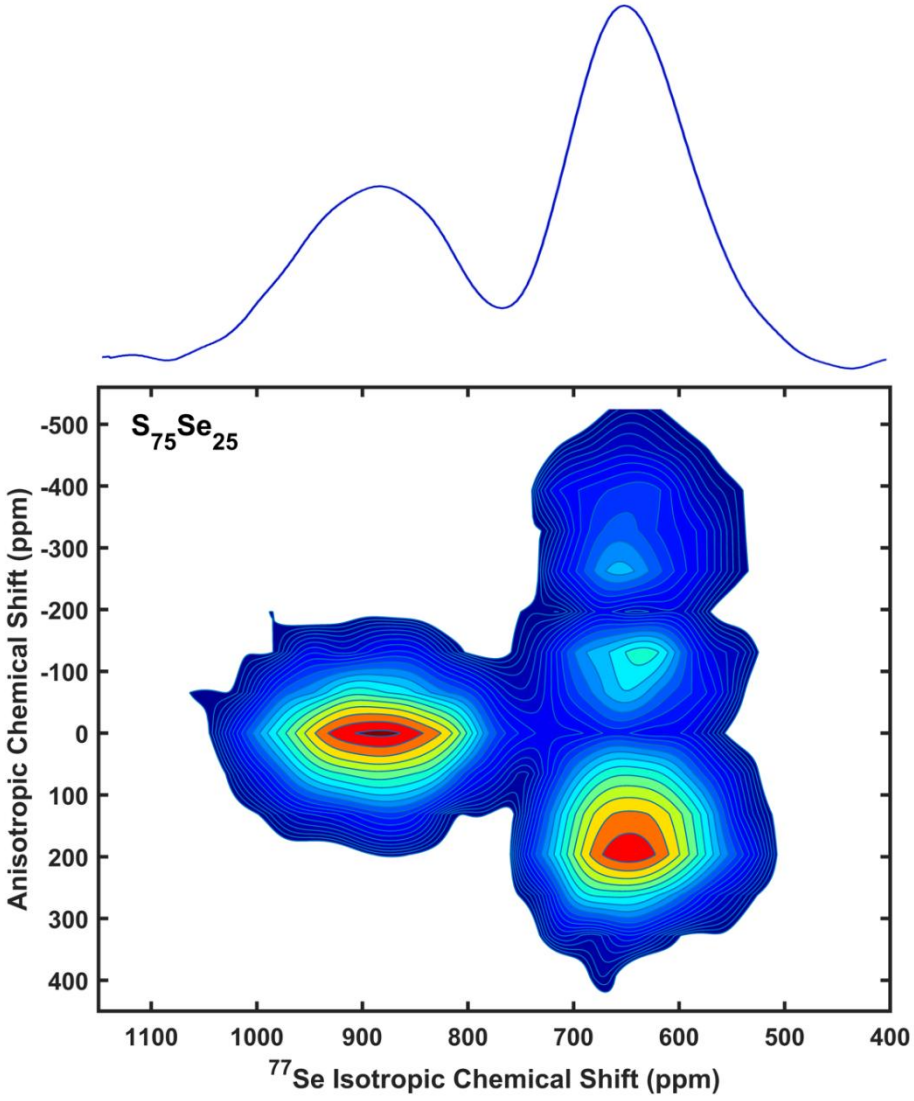
S75Se25
Anisotropic Chemical Shift (ppm)
-500
-400
-300
-200
-100
0
100
200
300
400
1100
1000
900
800
700
600
500
400
77Se Isotropic Chemical Shift (ppm)

Figure 5

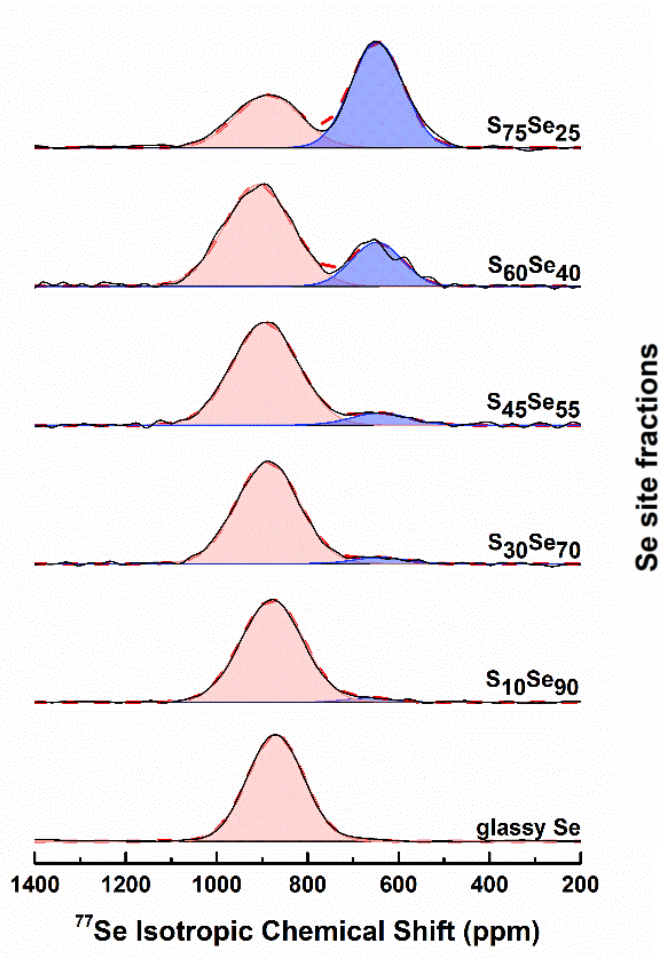
$S_{75}Se_{25}$
$S_{60}Se_{40}$
$S_{45}Se_{55}$
$S_{30}Se_{70}$
$S_{10}Se_{90}$
glassy Se
1400
1200
1000
800
600
400
200
^{77}Se Isotropic Chemical Shift (ppm)

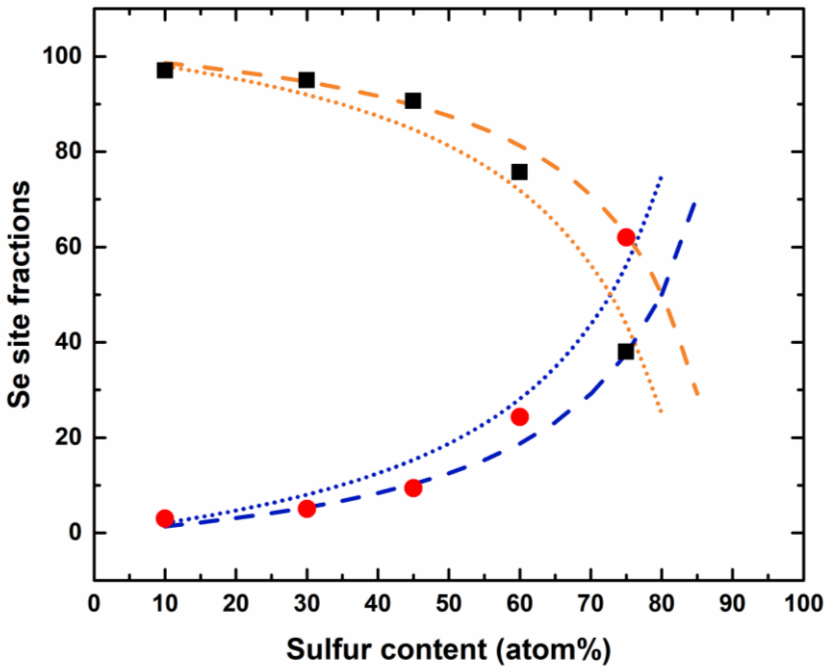
Se site fractions
0
20
40
60
80
100
0
10
20
30
40
50
60
70
80
90
100
Sulfur content (atom%)

Figure 6

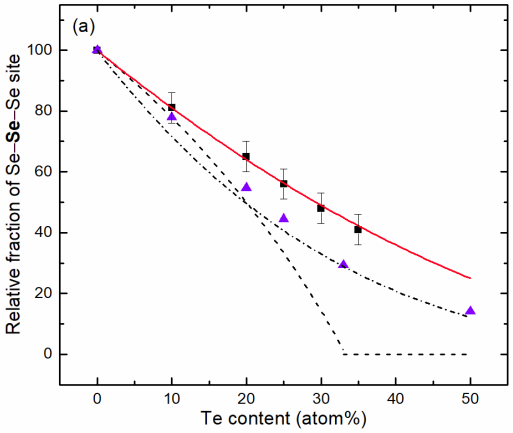
(a)
Relative fraction of Se–Se–Se site
Te content (atom%)

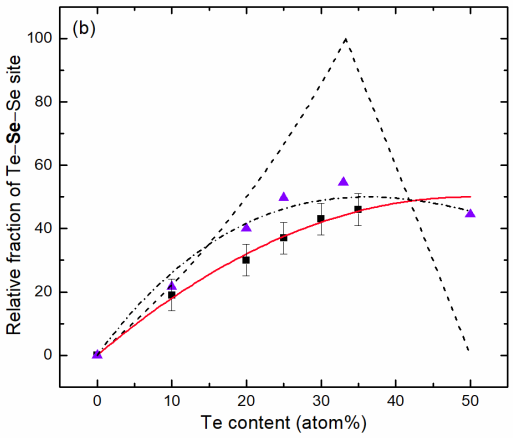
(b)
Relative fraction of Te–Se–Se site
Te content (atom%)

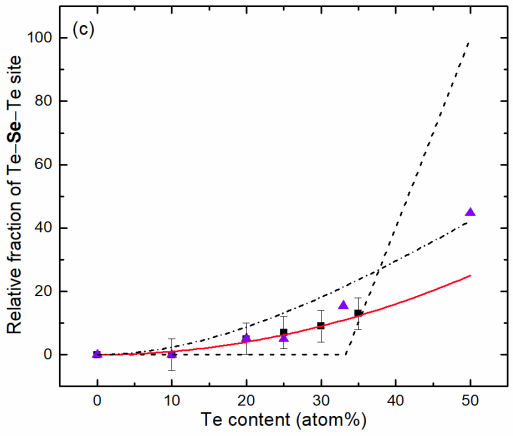
(c)
Relative fraction of Te–Se–Te site
Te content (atom%)

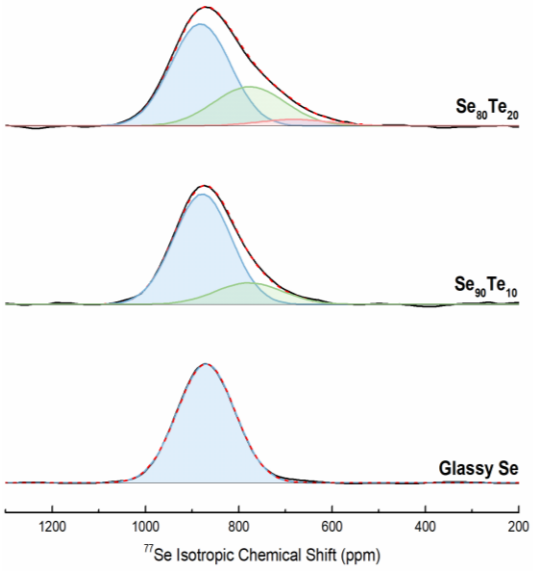
Se80Te20
Se90Te10
Glassy Se
77Se Isotropic Chemical Shift (ppm)

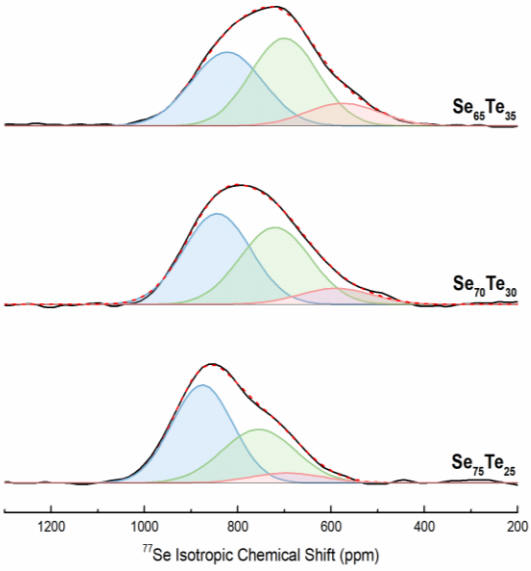
Se65Te35
Se70Te30
Se75Te25
77Se Isotropic Chemical Shift (ppm)

Figure 7

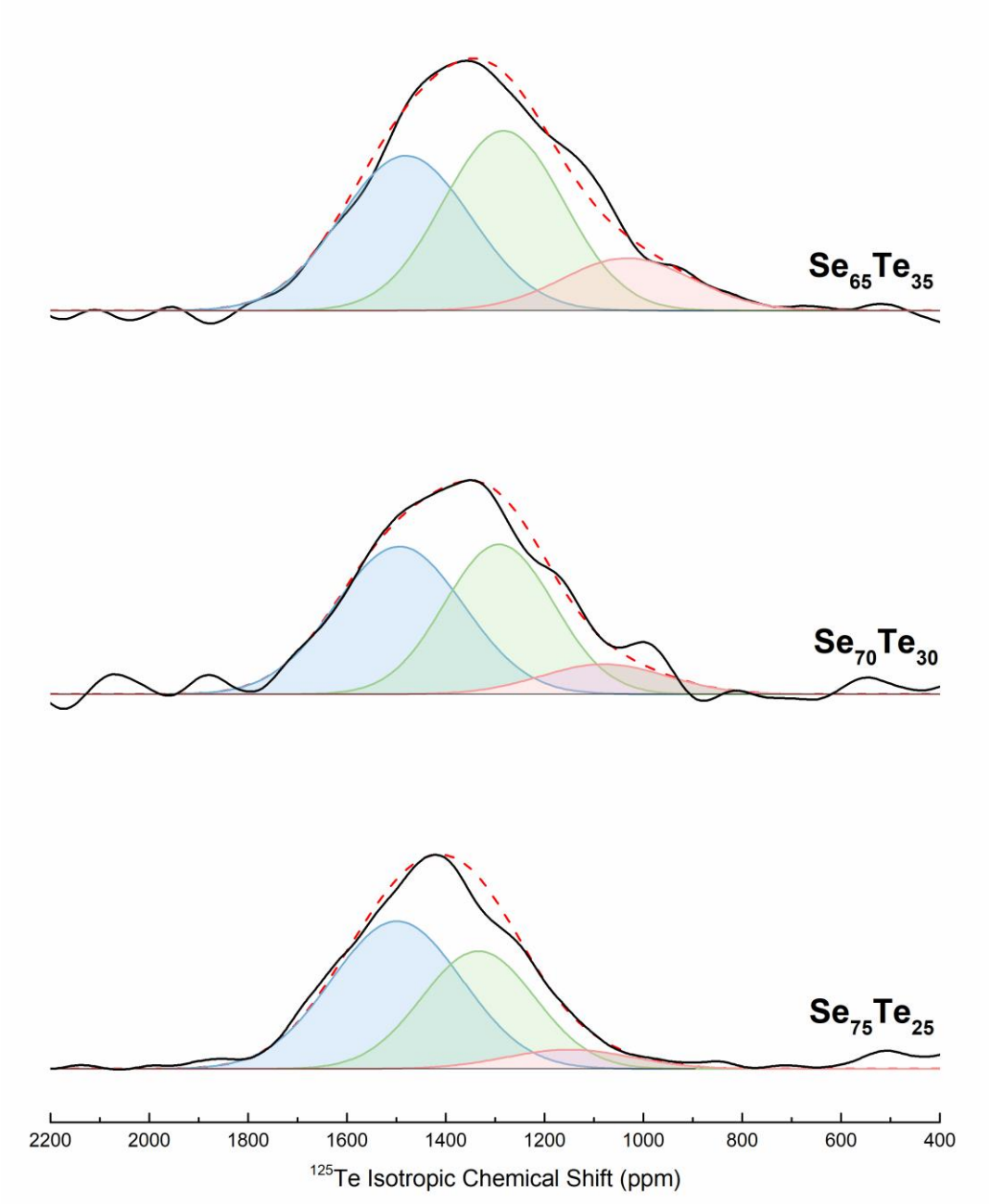
Se65Te35
Se70Te30
Se75Te25
2200
2000
1800
1600
1400
1200
1000
800
600
400
125Te Isotropic Chemical Shift (ppm)

Figure 8

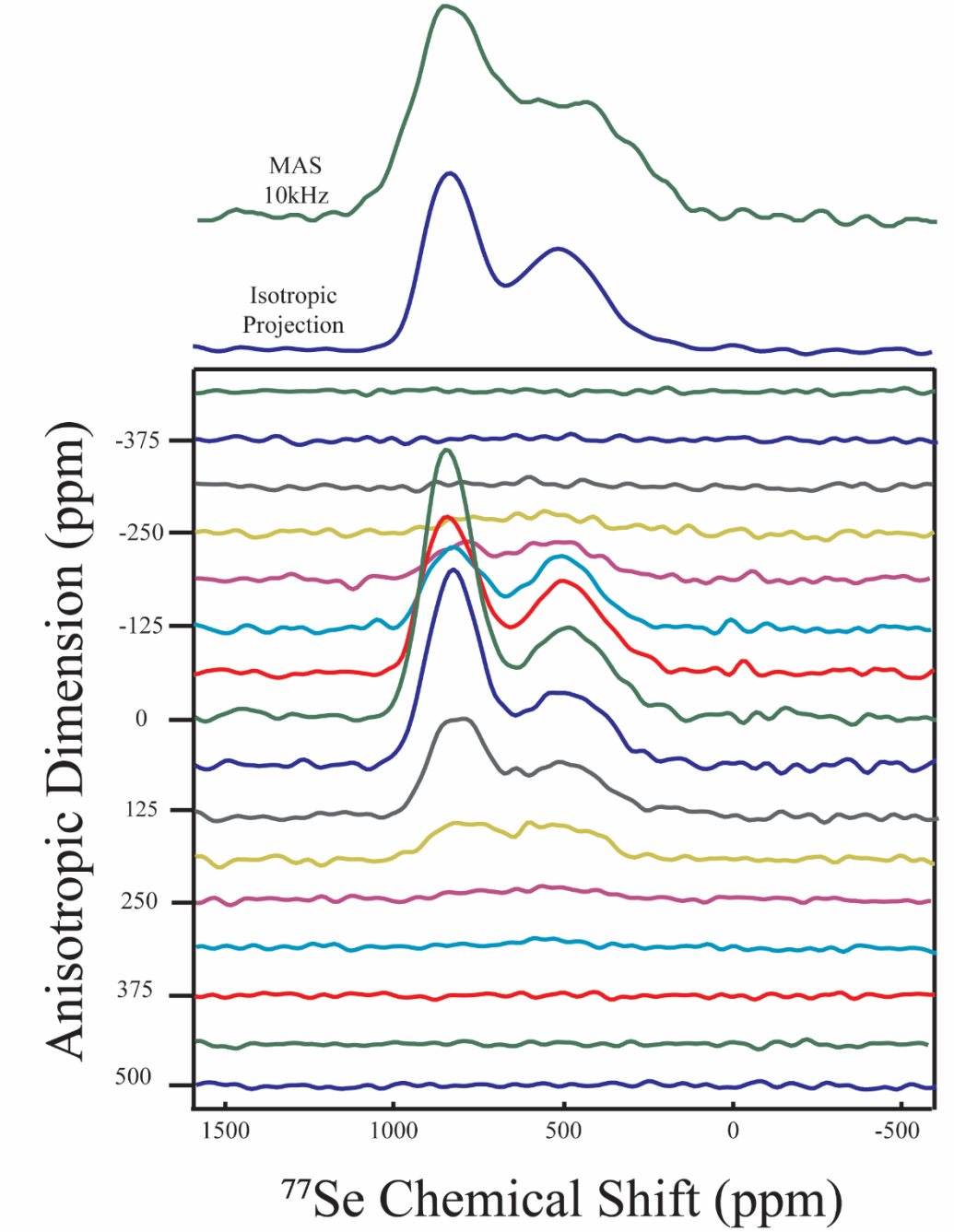
MAS
10kHz
Isotropic
Projection
Anisotropic Dimension (ppm)
-375
-250
-125
0
125
250
375
500
1500
1000
500
0
-500
77Se Chemical Shift (ppm)

Figure 9

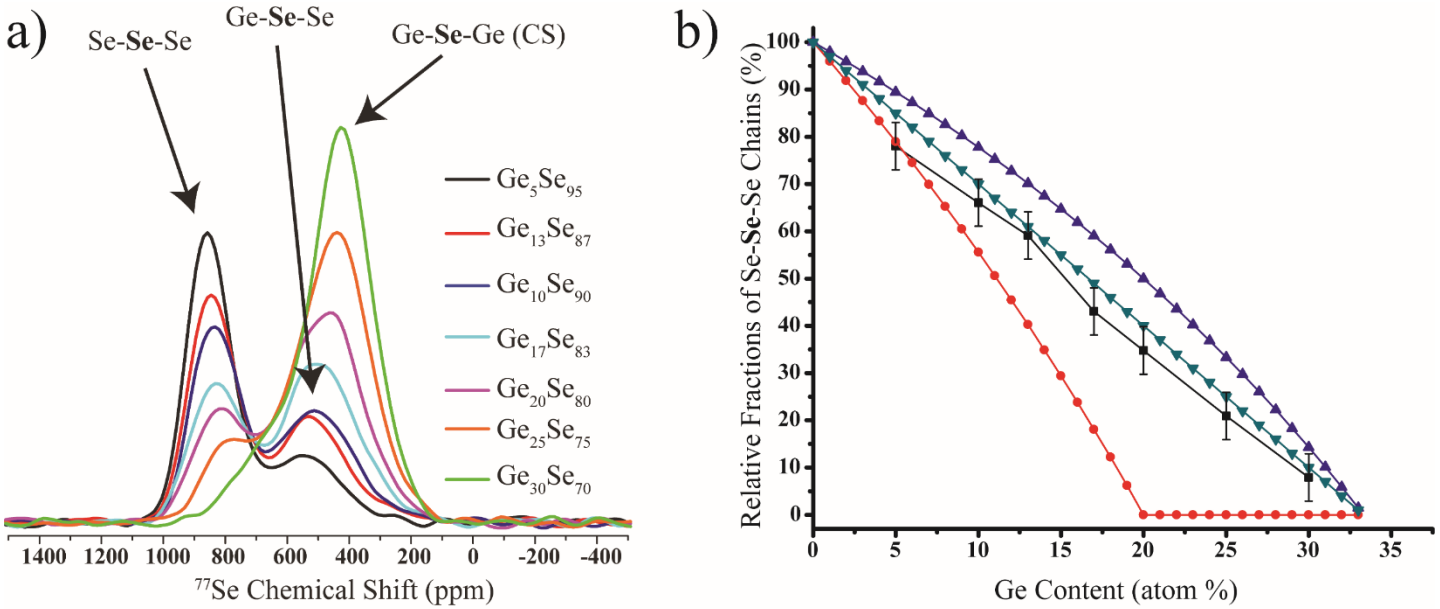
a)
Se-Se-Se
Ge-Se-Se
Ge-Se-Ge (CS)
Ge5Se95
Ge13Se87
Ge10Se90
Ge17Se83
Ge20Se80
Ge25Se75
Ge30Se70
1400 1200 1000 800 600 400 200 0 -200 -400
77Se Chemical Shift (ppm)
b)
Relative Fractions of Se-Se-Se Chains (%)
0 10 20 30 40 50 60 70 80 90 100
0 5 10 15 20 25 30 35
Ge Content (atom %)

Figure 10

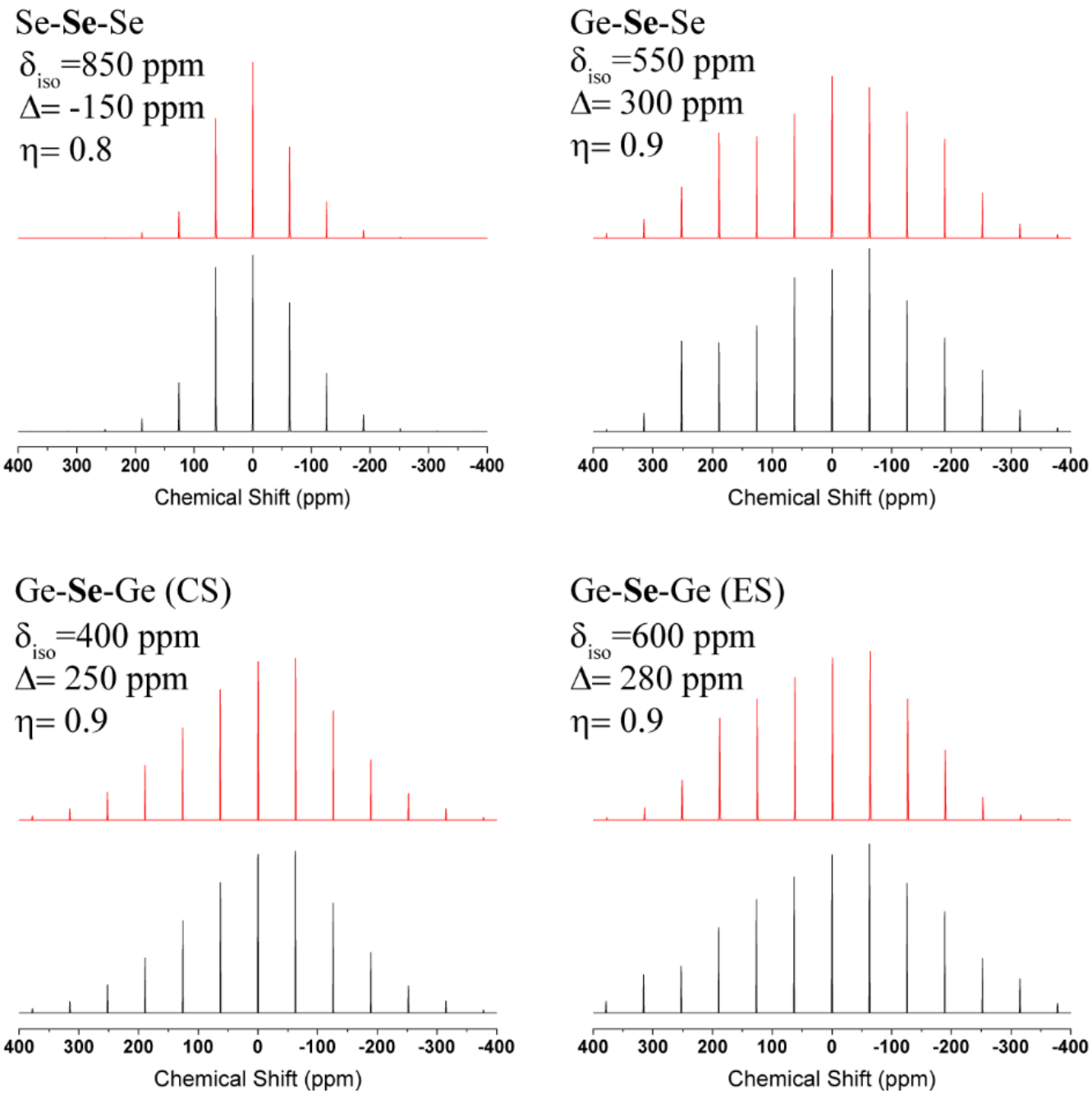
Se-Se-Se
δiso=850 ppm
Δ= -150 ppm
η= 0.8
Ge-Se-Se
δiso=550 ppm
Δ= 300 ppm
η= 0.9
Ge-Se-Ge (CS)
δiso=400 ppm
Δ= 250 ppm
η= 0.9
Ge-Se-Ge (ES)
δiso=600 ppm
Δ= 280 ppm
η= 0.9
400 300 200 100 0 -100 -200 -300 -400
Chemical Shift (ppm)

Figure 11

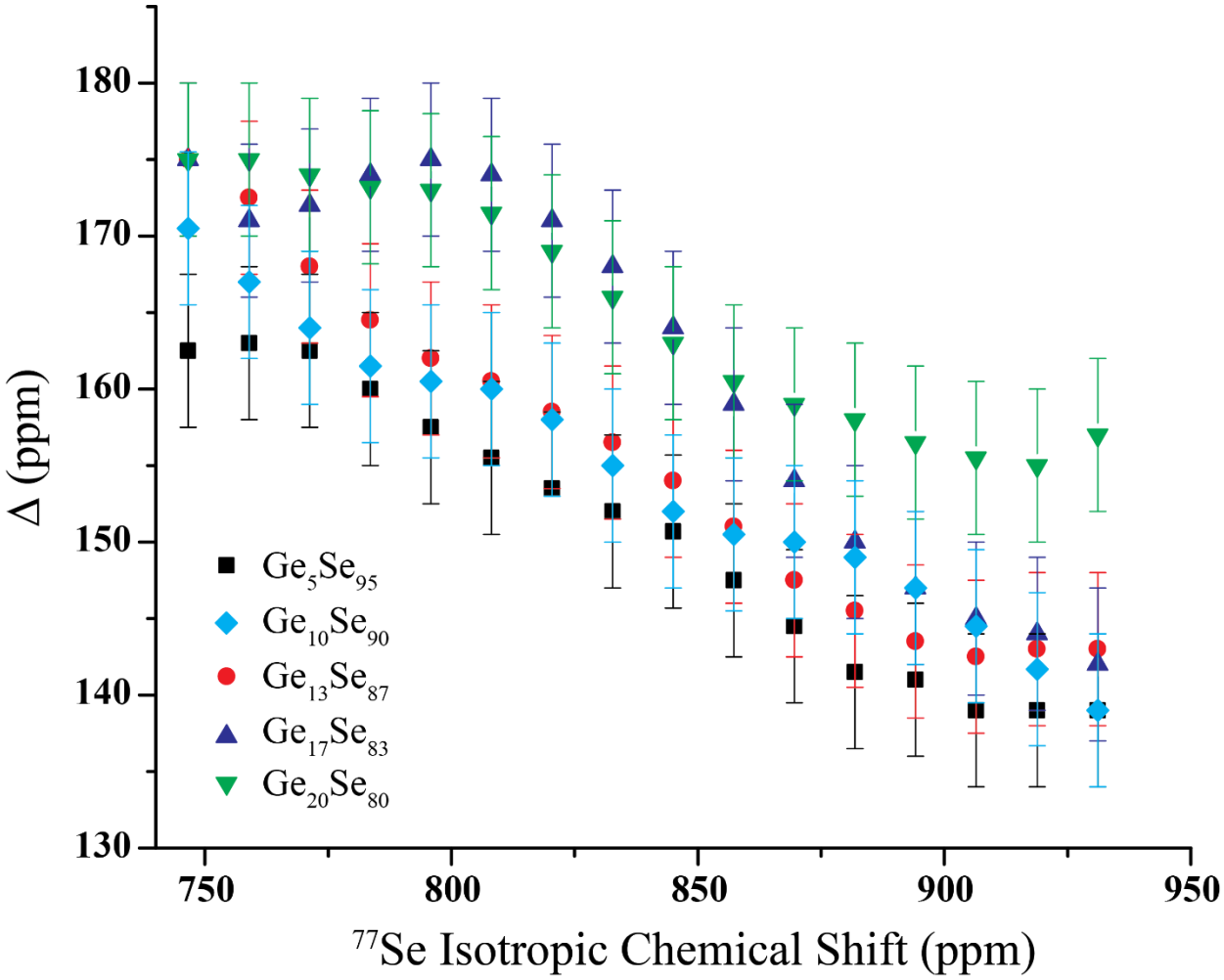
180
170
160
150
140
130
Δ (ppm)
750
800
850
900
950
77Se Isotropic Chemical Shift (ppm)
Ge5Se95
Ge10Se90
Ge13Se87
Ge17Se83
Ge20Se80

Figure 12

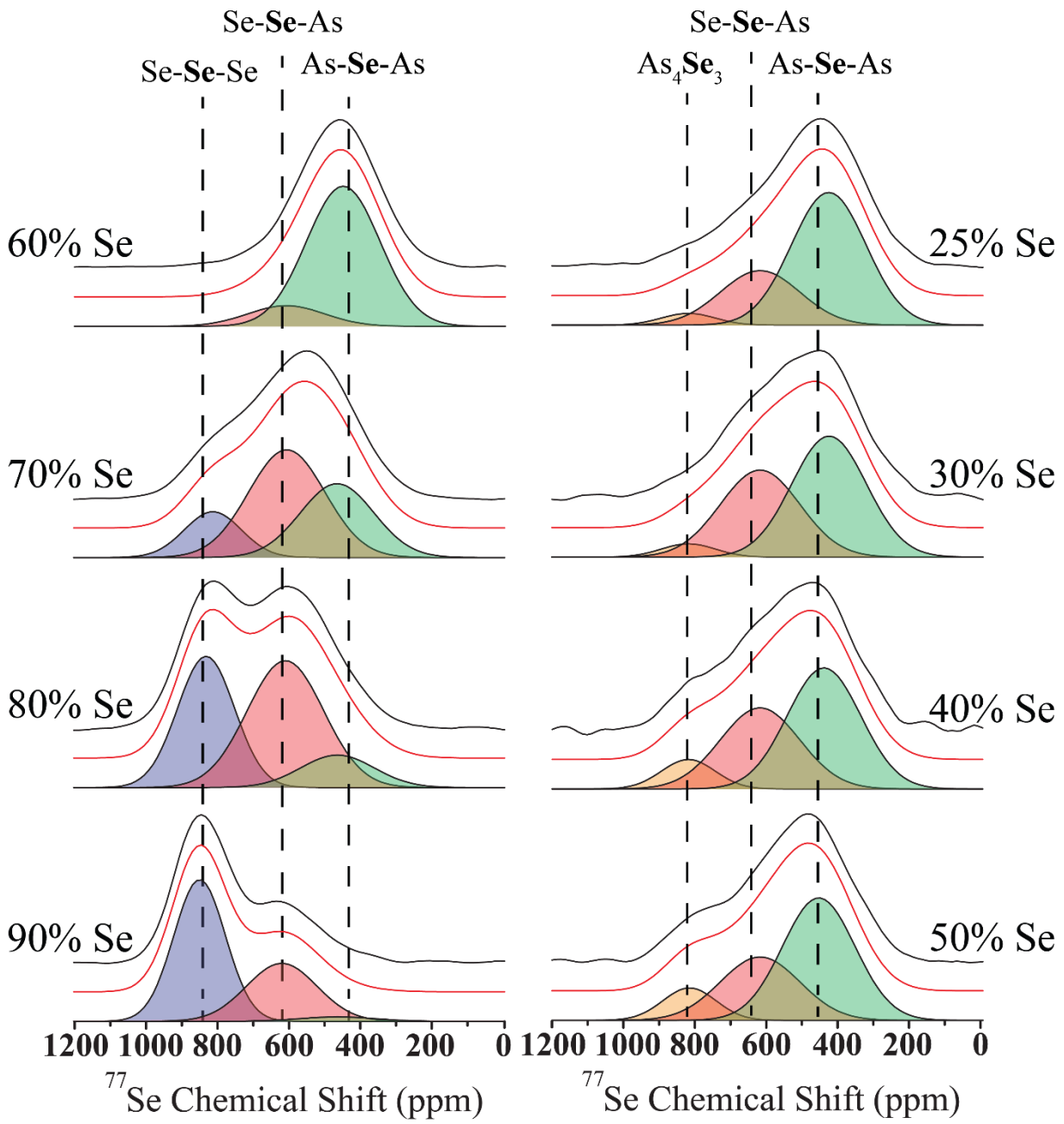
Se-Se-As
Se-Se-Se
As-Se-As
60% Se
70% Se
80% Se
90% Se
1200 1000 800 600 400 200 0
77Se Chemical Shift (ppm)
Se-Se-As
As4Se3
As-Se-As
25% Se
30% Se
40% Se
50% Se
1200 1000 800 600 400 200 0
77Se Chemical Shift (ppm)

Figure 13

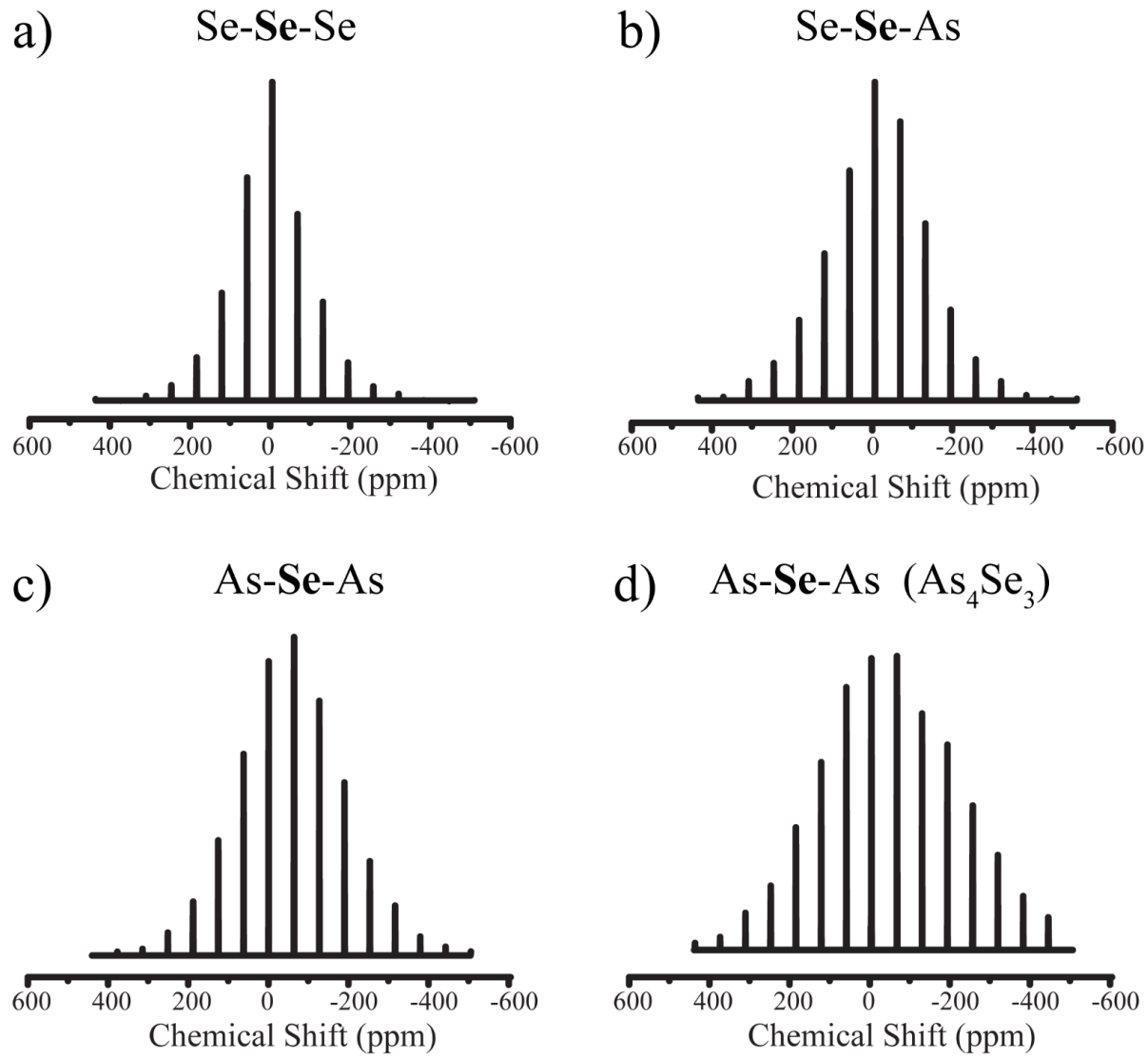
a)
Se-**Se**-Se
600 400 200 0 -200 -400 -600
Chemical Shift (ppm)
b)
Se-**Se**-As
600 400 200 0 -200 -400 -600
Chemical Shift (ppm)
c)
As-**Se**-As
600 400 200 0 -200 -400 -600
Chemical Shift (ppm)
d)
As-**Se**-As (As_4Se_3)
600 400 200 0 -200 -400 -600
Chemical Shift (ppm)

Figure 14

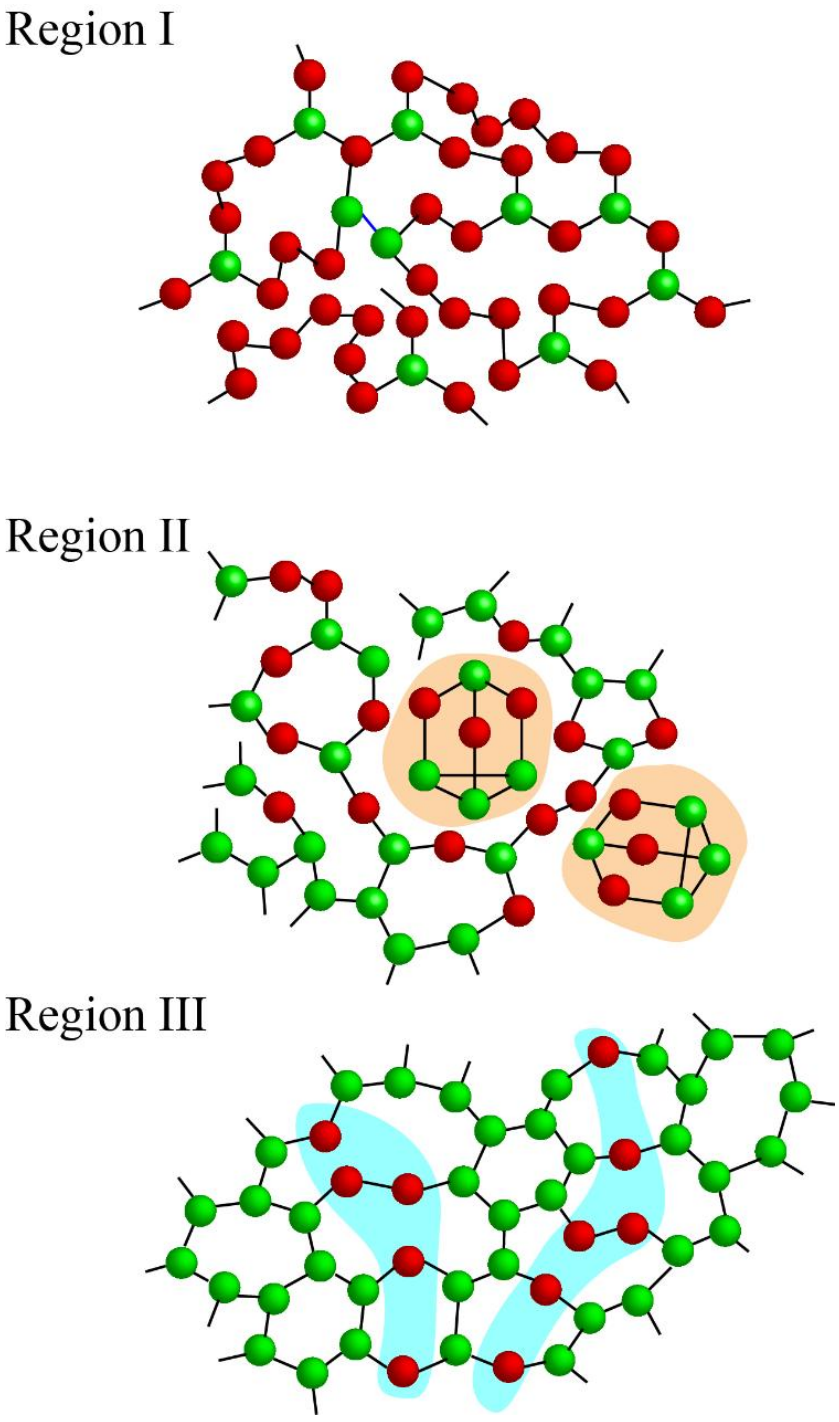

Figure 15

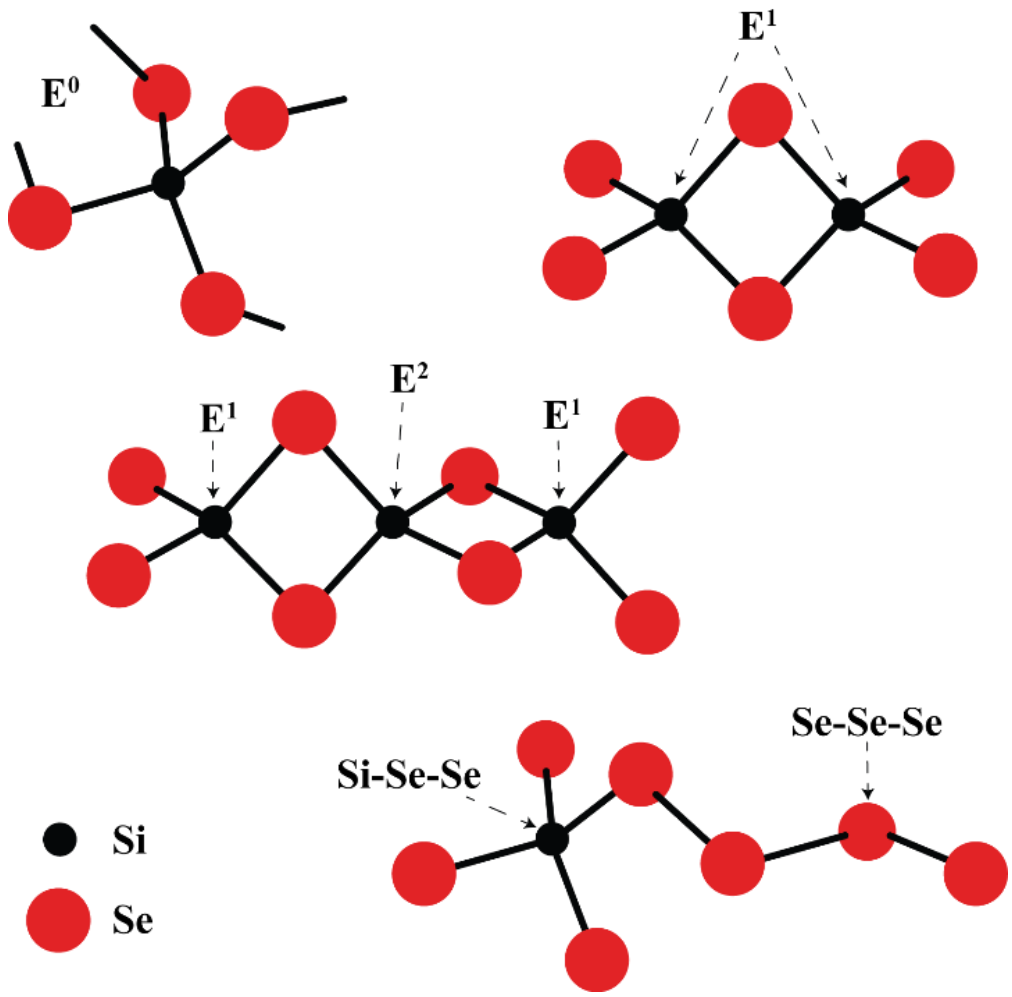

Figure 16

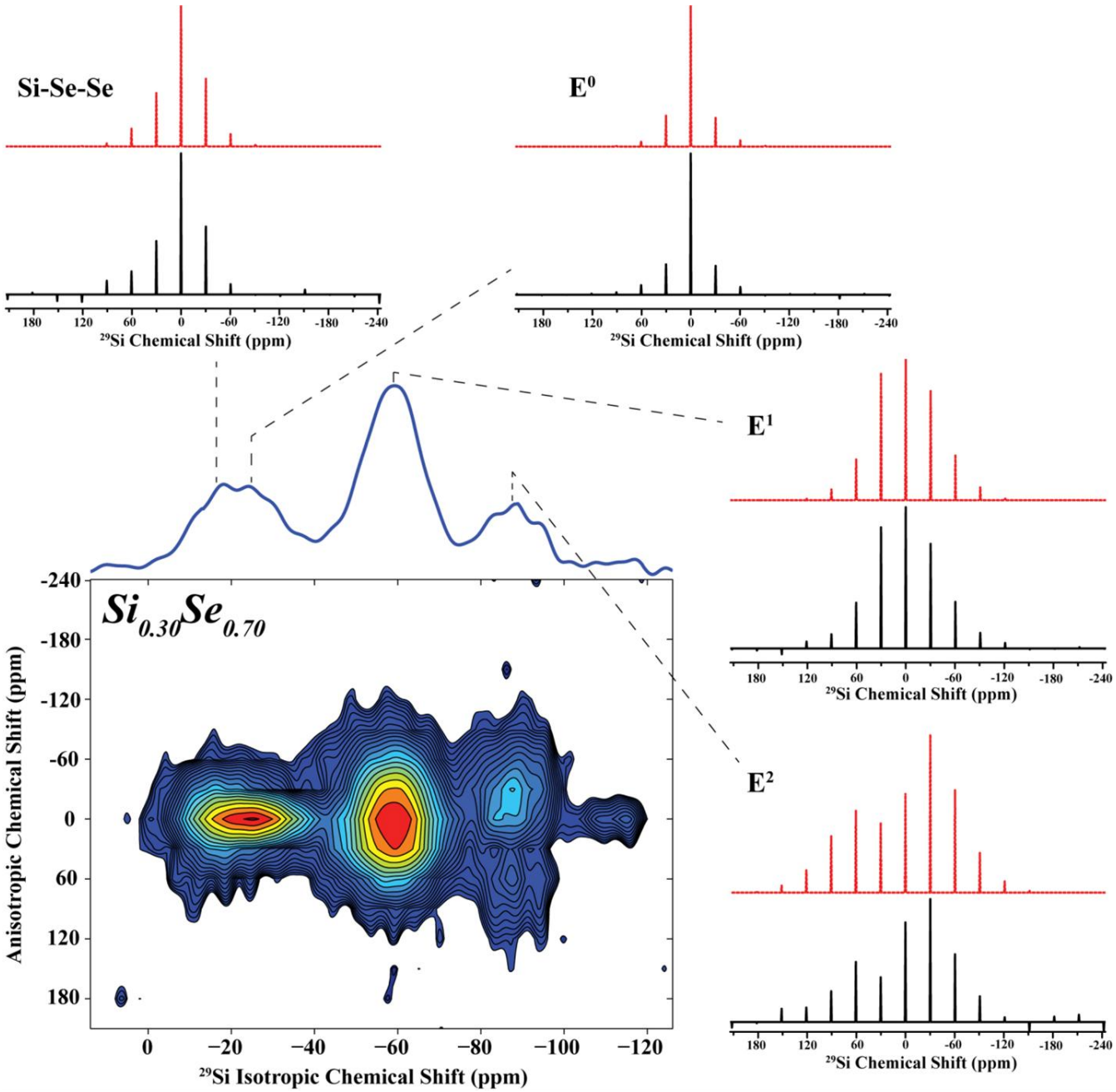
Si-Se-Se
E⁰
E¹
E²
180 120 60 0 -60 -120 -180 -240
²⁹Si Chemical Shift (ppm)
Si0.30Se0.70
Anisotropic Chemical Shift (ppm)
-240 -180 -120 -60 0 60 120 180
0 −20 −40 −60 −80 −100 −120
²⁹Si Isotropic Chemical Shift (ppm)

Figure 17

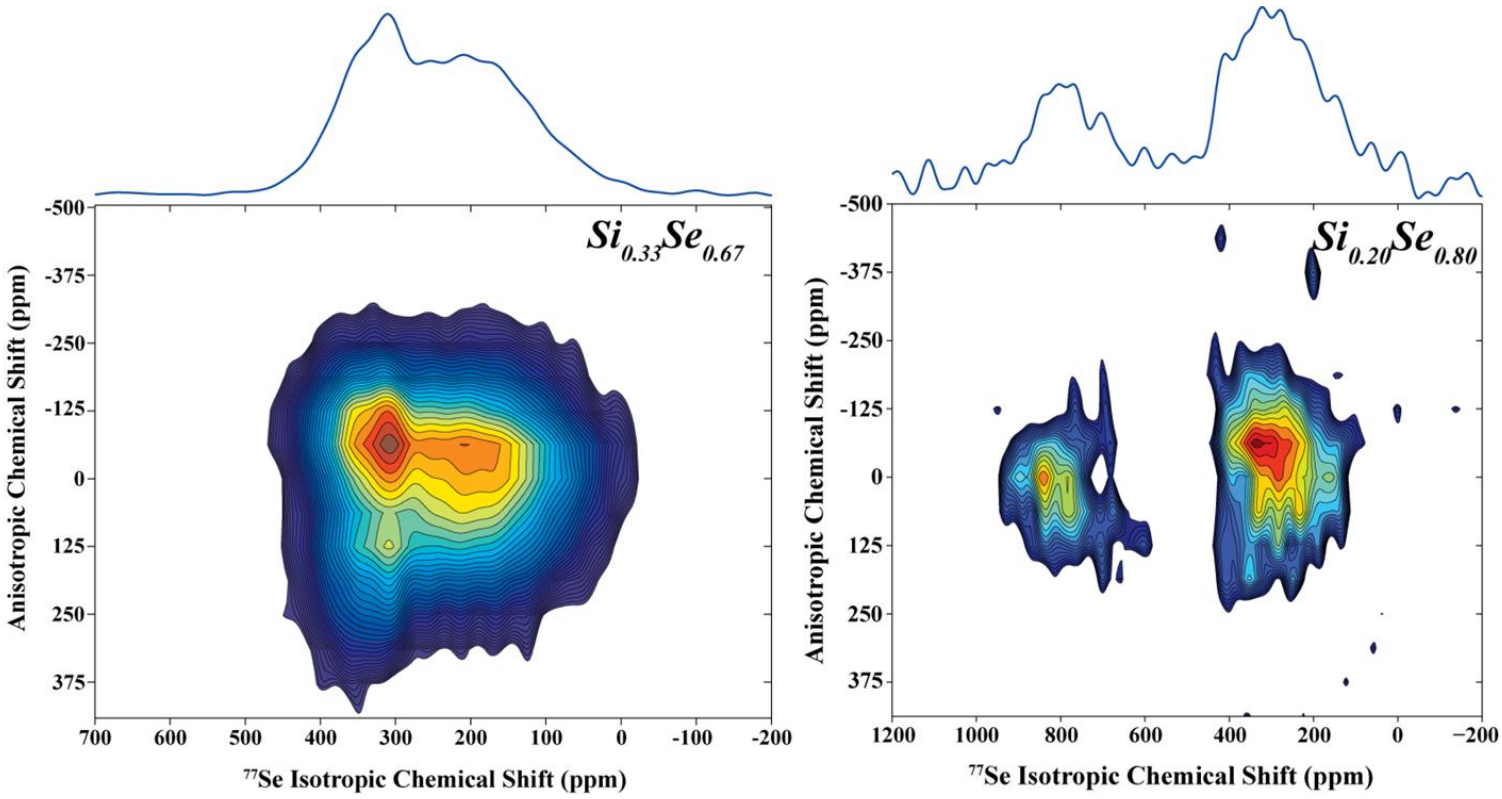
Si0.33Se0.67
Si0.20Se0.80
Anisotropic Chemical Shift (ppm)
77Se Isotropic Chemical Shift (ppm)
-500
-375
-250
-125
0
125
250
375
700
600
500
400
300
200
100
0
-100
-200
1200
1000
800
600
400
200
0
−200

Figure 18

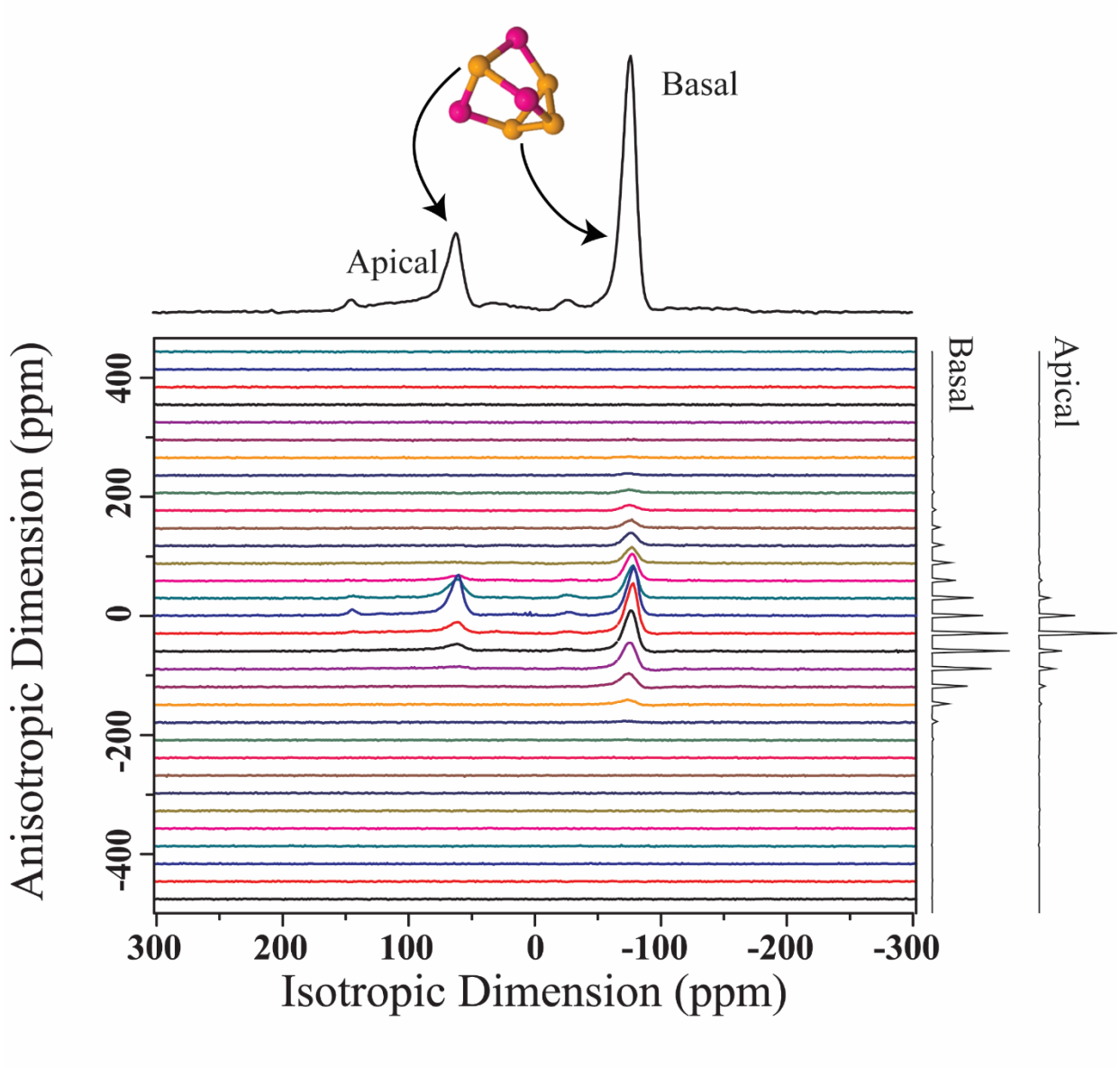
Basal
Apical
Anisotropic Dimension (ppm)
400
200
0
-200
-400
Basal
Apical
300
200
100
0
-100
-200
-300
Isotropic Dimension (ppm)

Figure 19

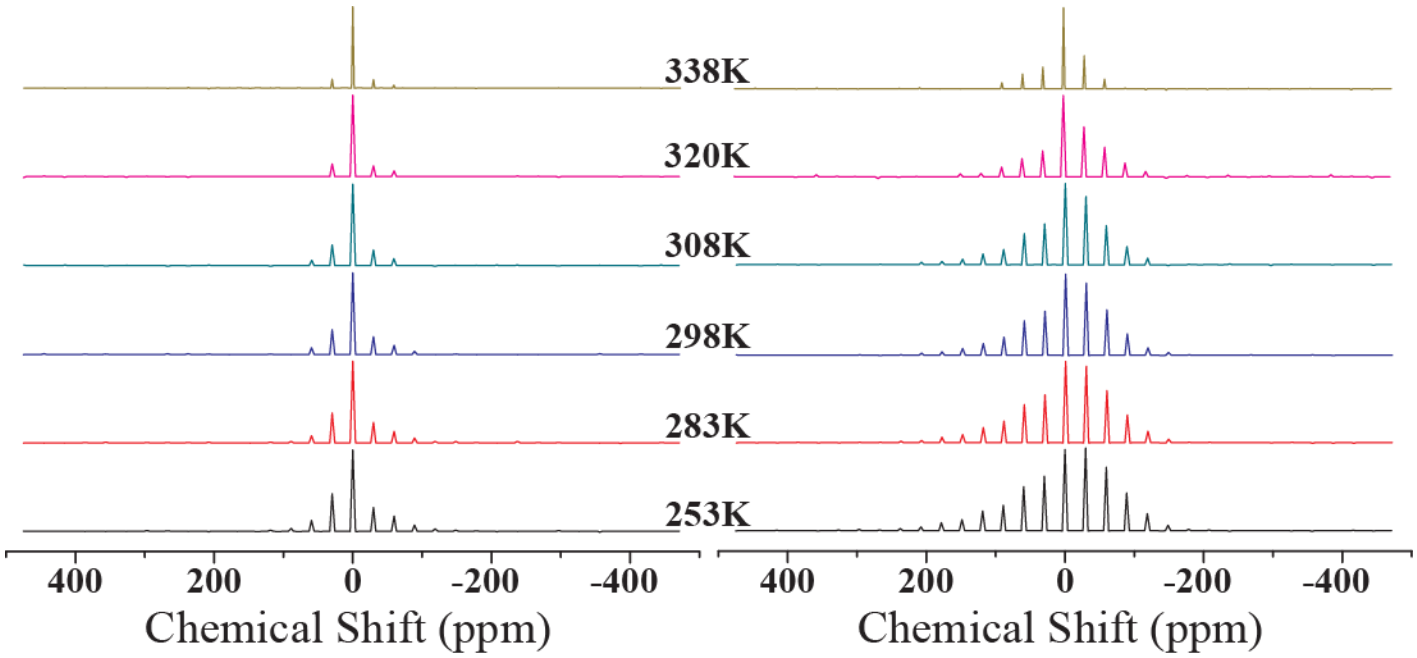
338K
320K
308K
298K
283K
253K
400
200
0
-200
-400
Chemical Shift (ppm)
400
200
0
-200
-400
Chemical Shift (ppm)

Figure 20

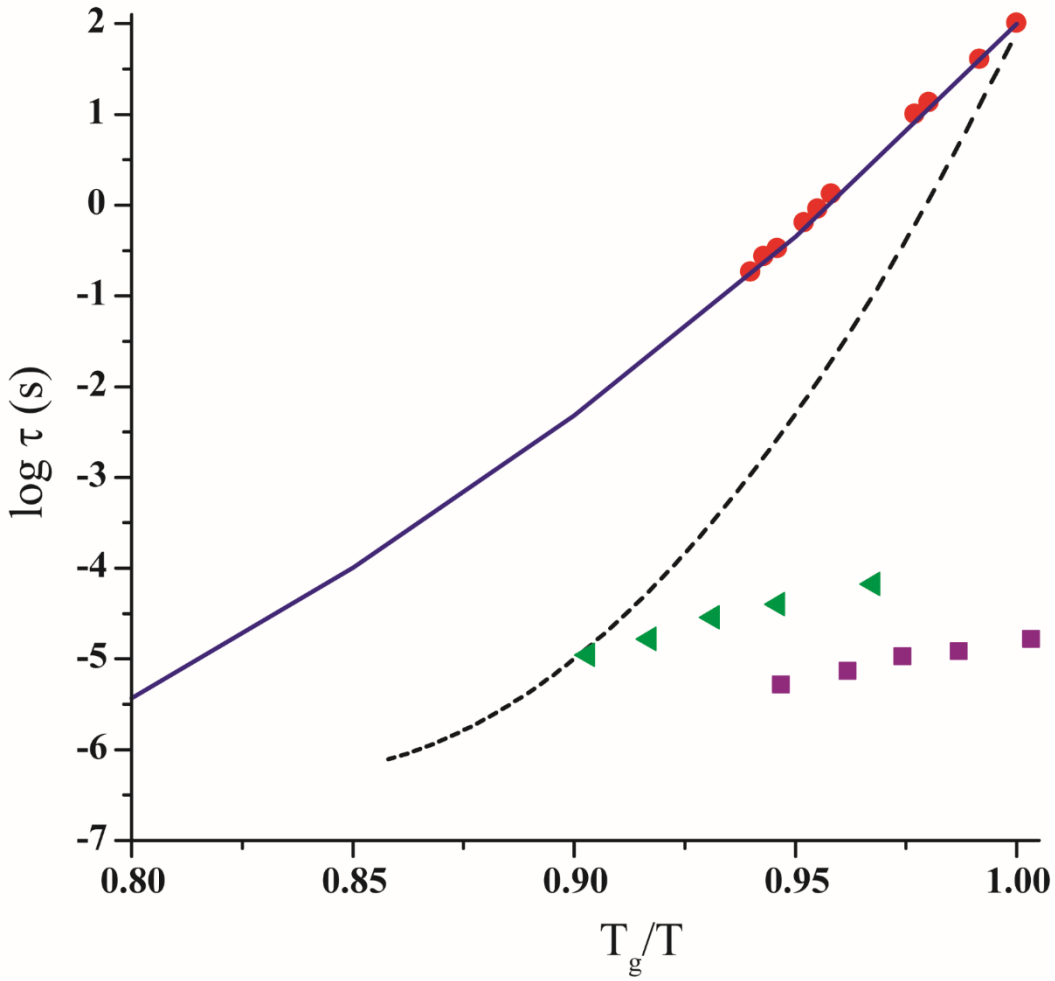

Credit Author Statement:

Derrick Kasemen: Wrote part of the manuscript. **Sabyasachi Sen**: Conceived the project, provided supervision and wrote part the manuscript.

***Declaration of Interest Statement**

Declaration of interests

☒ The authors declare that they have no known competing financial interests or personal relationships that could have appeared to influence the work reported in this paper.

☐The authors declare the following financial interests/personal relationships which may be considered as potential competing interests: